Biophysical Journal
Article

Biophysical Society

Engineered Passive Potassium Conductance in the KR2 Sodium Pump

Arend Vogt,[1] Arita Silapetere,[1] Christiane Grimm,[1] Florian Heiser,[1] Maximiliano Ancina Möller,[1] and Peter Hegemann[1,*]
[1]Institute of Biology, Experimental Biophysics, Humboldt-Universität zu Berlin, Berlin, Germany

ABSTRACT Light-driven sodium pumps (NaRs) are microbial rhodopsins that utilize light energy to actively transport sodium ions out of the cell. Here, we used targeted mutagenesis and electrophysiological methods in living cells to demonstrate that NaRs can be converted into light-activated cation channels by molecular engineering. Specifically, introduction of the R109Q mutation into the sodium ion pump of *Dokdonia eikasta* (KR2) results in passive ion conductance, with a high preference for potassium over sodium ions. However, in this mutant, residual active outward pumping of sodium ions competes with passive inward transport of potassium. Channel-like behavior could also be achieved by introduction of other mutations into the KR2 counterion complex, and further, these modifications were transferrable to other NaRs. Combining the R109Q replacement with modifications at position S70 removed the residual sodium pumping and greatly enhanced the channel-like activity. However, passive photocurrents were only observed in leak mutants if the KR2 counterions, D116 and D251, were deprotonated, which was only observed under alkaline conditions. Overall, our results reveal that interactions between R109 and the nearby residues, L75, S70, D116, and D251, prevent passive backflow during ion transport in NaRs.

INTRODUCTION

Microbial rhodopsins are light-sensitive proteins, containing seven-transmembrane domains, that are found in archaea, bacteria, and lower eukaryotes. These function as ion transporters, sensors, or enzymes, using covalently bound retinal as a light-sensitive chromophore (1). Light-gated ion channels (channelrhodopsins) and light-driven ion pumps are widely used in neuroscience to noninvasively investigate and manipulate neuronal activity with light (2–4). In addition to their optogenetic applicability, microbial rhodopsins offer an excellent opportunity to investigate the structural differences between channels and pumps and to elucidate how these differences affect the function of ion transporters (5). The high similarity between channels and pumps of the microbial rhodopsin family was initially noted with the discovery of the first channelrhodopsins (6–8), but only recently have active proton pumps been converted into passive proton channels by the introduction of specific mutations or synthetic chromophores (9–11). In 2013, the family of ion-pumping rhodopsins was further expanded by the discovery of light-driven Na^+ pumps (NaRs) (12–14). These cation pumps further raised the question as to whether the structural mechanisms existing in proton pumps to prevent passive proton leakage are also preserved in sodium pumps. This question is challenging because both proton and sodium pumps differ in several respects. Proton pumps contain water molecules and residues, which are stepwise protonated and deprotonated, and the released proton is already bound in the dark state (1). In contrast, in sodium pumps, the same sodium ion has to enter and leave the protein during the photocycle (14–16).

Here, we assessed the potential for converting NaRs into channel-like cation transporters using mutations that are known to induce passive currents in proton pumps (Fig. 1 *A*). Introduction of these leak mutations into the sodium ion pump of *Dokdonia eikasta* (KR2) resulted in inward-directed photocurrents at physiological electrochemical loads, as observed by two-electrode voltage-clamp (TEVC) measurements in *Xenopus laevis* oocytes. These photocurrents were identified as light-controlled passive cation conductance. Notably, we found that the mutant KR2-R109Q promotes inward photocurrents and is highly

Submitted December 20, 2018, and accepted for publication April 3, 2019.

*Correspondence: hegemann@rz.hu-berlin.de

Christiane Grimm's present address is NeuroTechnology Center, Department of Biological Sciences, Columbia University, New York, New York 10027.

Editor: Ian Forster.

https://doi.org/10.1016/j.bpj.2019.04.001

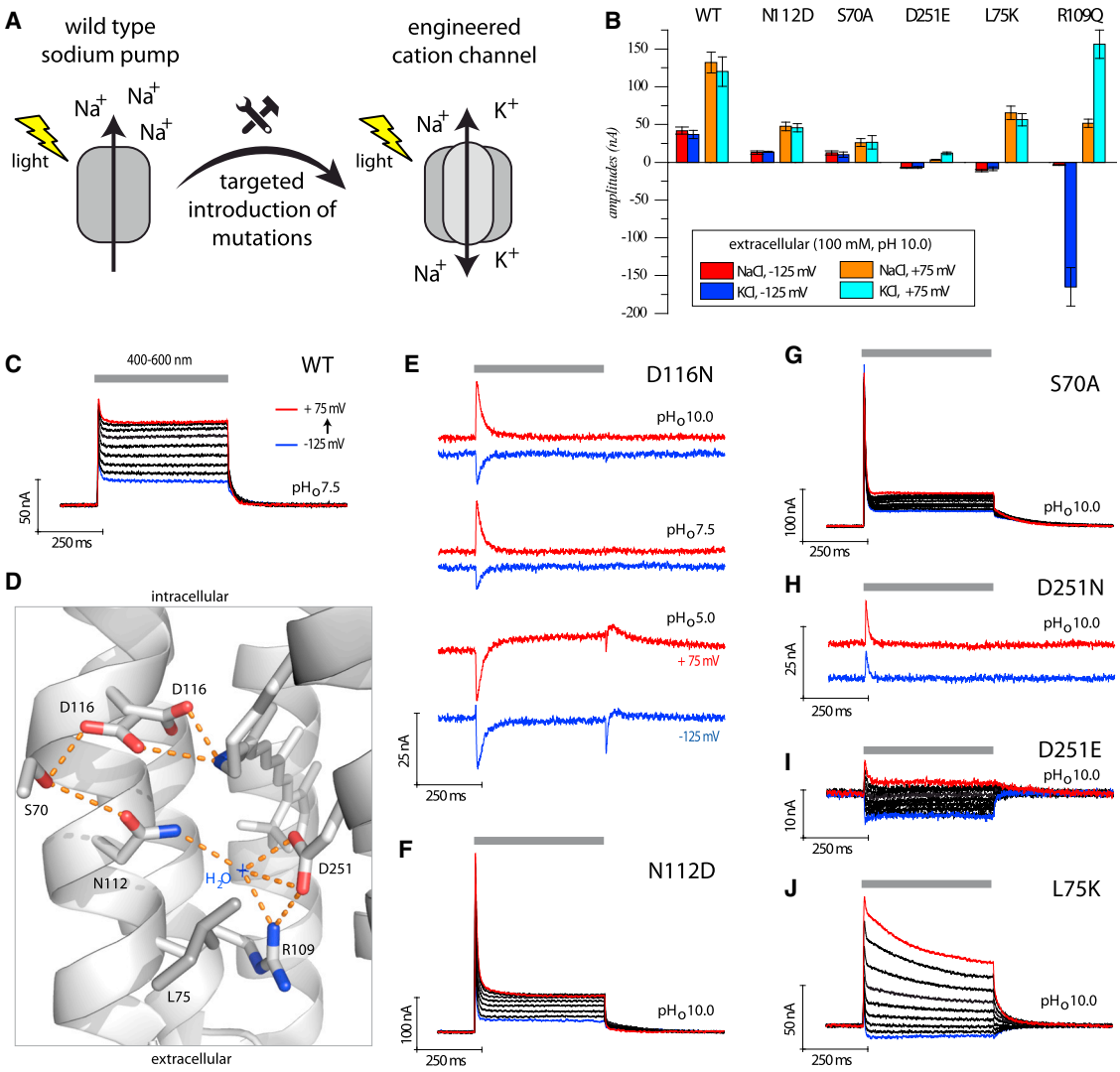

FIGURE 1 Electrophysiological analysis of KR2$_{\beta HK}$ in *X. laevis* oocytes. (*A*) A sketch about the intention of this scientific work is shown. (*B*) Quantitative comparison of the stationary photocurrent amplitudes (see Fig. S6 *A* for details). (*C*) Representative photocurrent traces of wild-type (WT) KR2 at $pH_o = 7.5$ and different holding potentials (in 25 mV steps) are shown. (*D*) The KR2 crystal structure (PDB: 3X3C) at neutral pH is shown, illustrating the mutated positions of the counterion complex. (*E*) Substitution of the proposed primary proton acceptor (D116N) causes pH_o-dependent transient photocurrents. Traces at −125 mV (*blue*) and +75 mV (*red*) for each pH_o value are displayed. (*F–J*) Photocurrents of additional mutants are shown at $pH_o = 10$. All traces were measured in extracellular buffer containing 100 mM NaCl. Oocytes were illuminated with 500 ms light pulses, using a xenon lamp and a 400–600 nm broadband filter. To see this figure in color, go online.

selective for potassium over sodium. This observation is particularly intriguing because of the fact that light-gated potassium-selective channels are a valuable optogenetic tool for the inhibition of neuronal activity.

MATERIALS AND METHODS

Molecular biology

We utilized the pGEMHE vector for expression in oocytes (T7-promotor, polyadenylation site), the pmKate2-N1 plasmid for expression in ND7/23 cells (CMV promotor), and the pET21a + vector for expression in *Escherichia coli*. Site-directed mutagenesis was performed using the QuikChange Kit (Agilent Technologies, Santa Clara, CA). NaRs containing specific targeting sequences were codon-optimized and synthesized by GenScript (Piscataway Township, NJ), using human-optimized codons for oocytes and ND7/23 cells and *E. coli*-optimized codons for pH assays and protein purification. Protein IDs for all tested NaRs are shown in Fig. S1 *A*, and a multiple sequence alignment is shown in Fig. S2 (prepared with Clustal Omega, European Molecular Biology Laboratory). The detailed sequences for all KR2 constructs are shown in Fig. S3.

TEVC measurements in *X. laevis* oocytes

Protocols for animal maintenance and oocyte harvesting were approved by the German administration for animal testing (Berlin, Germany). Female frogs were maintained in tap water at 18°C with a 12:12 h light/dark cycle. Frogs were anesthetized with 2 g/L tricaine (Sigma Aldrich, St. Louis, MO) for harvest of ovary lobes. Oocytes were then washed and stored in oocyte incubation buffer at 4°C (96 mM NaCl, 5 mM KCl, 2 mM $CaCl_2$, 1 mM

$MgCl_2$, 5 mM 3-(*N*-morpholino)propanesulfonic acid, 50 U penicillin/streptomycin (pH 7.5)). For injection, oocytes were first defolliculated by hand, after partial digestion with 2 mg/L collagenase solution (dissolved in antibiotic- and Ca^{2+}-free oocyte incubation buffer), for 1.5 h at 18°C. Oocytes were then injected with 30 ng capped messenger RNA using the Nanoliter 2000 microinjection system (World Precision Instruments, Sarasota, FL) and incubated at 18°C for 4 days. This capped messenger RNA was synthesized in vitro from *NheI*-linearized pGEMHE plasmid, using the mMESSAGE mMACHINE T7 Kit (Life Technologies, Carlsbad, CA). After injection, the incubation buffer was supplemented with 5 μM all-*trans* retinal (Sigma Aldrich).

TEVC experiments were performed using a Turbo TEC-10X amplifier without transient compensation (npi electronic, Tamm, Germany). Buffer composition is shown in Fig. S4. Continuous light was provided by an XBO75/2 75 W xenon lamp (Carl Zeiss, Oberkochen, Germany) and was controlled by an LS3 shutter (Vincent Associates UNIBLITZ Shutter Systems, Rochester, NY). Light was passed through a 400–600 nm broadband filter (Optics Balzers, Liechtenstein, Germany), with an intensity of 10 mW/mm^2. Microelectrodes were fabricated from borosilicate glass capillaries (1.50 mm outer diameter and 1.17 mm inner diameter; Harvard Apparatus, Holliston, MA), using a P-97 micropipette puller (Sutter Instrument, Novato, CA), and microelectrode resistance was maintained between 0.6 and 2.0 MΩ. Data acquisition and light triggering were controlled using the Axon pCLAMP 9.0 software via the Digidata 1322A interface (Molecular Devices, San Jose, CA). Currents were recorded at 10 kHz and filtered to 1 kHz using built-in circuits. The photocurrent traces were baseline corrected and filtered to 300 Hz (Gaussian low-pass cutoff filter, using pCLAMP). Reversal potentials (E_{rev}) were estimated for each single buffer condition by linear regression. For current-voltage plots, measurements from each single oocyte (and ND7/23 cells) were normalized to a reference condition (indicated with *small black boxes* in the figures and in the legends). All normalized values from several cells are summarized and are shown as mean ± standard error.

Patch-clamp recordings with ND7/23 cells

ND7/23 cells were cultured in Dulbecco's modified Eagle's medium, supplemented with 5% (v/v) fetal bovine serum and 1 μg/mL penicillin/streptomycin at 37°C under a 5% CO_2 atmosphere. For all experiments, 5×10^4 cells/mL were seeded in dishes on poly-D-lysine-coated glass coverslips in media supplemented with 1 μM all-*trans* retinal (Sigma Aldrich). The following day, cells were transiently transfected using FuGENE HD Transfection Reagent (Promega, Madison, WI). Electrophysiological recordings were conducted 24–30 h after transfection. Patch pipettes (2–3.5 MΩ) were prepared from standard wall (inner diameter 0.86 nm, outer diameter 1.50 nm) borosilicate capillaries with filament (Warner Instruments, Harnden, CT), using a micropipette puller (P1000; Sutter Instrument). The recordings were performed in the whole-cell configuration at room temperature. Light was provided by a CoolLED system (model pE-4000), coupled to the epifluorescence port of an Axiovert 100 TV inverted microscope (Carl Zeiss). Cells were illuminated with a 525 nm light-emitting diode (full width at half-maximum 31 nm), with a power of 23 mW/mm^2 in the focal plane. The currents were filtered at 5 kHz with an ELC-03XS amplifier (npi electronic) and digitized at a sampling rate of 20 kHz (Digidata 1440 A; Molecular Devices). Buffer composition is listed in Fig. S4. For stability reasons, the patch and following measurements were always initiated in the extracellular high-sodium buffer (NaCl 9.0). Electrophysiology data were analyzed using Clampfit 10.4 (Molecular Devices).

Monitoring light-induced pH changes in *E. coli* suspension (pH assay)

The expression plasmid (pET21a+) containing KR2-wild type (WT) or KR2-R109Q was transformed into *E. coli* C41 (DE3) cells. Protein expression was induced in cells at an optical density at 600 nm (OD_{600}) of 1.0 with 0.5 mM isopropyl β-D-1-thiogalactopyranocide (IPTG; Carl Roth, Karlsruhe, Germany), in lysogeny broth medium supplemented with 5 μM all-*trans* retinal (Sigma Aldrich). Induced cells were grown for 2.5 h at 37°C ($OD_{600} \approx 3.0$), followed by centrifugation for 10 min at 3000 × *g*. The pellets were then resuspended in salt solution (either 100 mM NaCl or 100 mM KCl, no further ingredients) for 1.5 h at room temperature. These cells were centrifuged again, and the pellets were resuspended in fresh salt solution (concentrated to $OD_{600} = 10$) and stored in the dark at room temperature until measurement.

For analysis of light-induced pH changes, the *E. coli* suspension (8 mL) was stirred in a temperature-controlled glass chamber (25°C). The pH was measured every 5 s (WTW model inoLab pH 730; Weilheim, Germany), and the cells were illuminated with white light from a slide projector (model Noris Trumpf Halogen 150; Ernst Plank KG, Germany). The first measurement was obtained without any ionophore, followed by a second measurement after addition of the protonophore, carbonyl cyanide m-chlorophenyl hydrazone (CCCP; Sigma Aldrich), at a final concentration of 50 μM.

Purification and spectroscopy of KR2

Expression plasmid transformation, protein expression, and protein purification were performed as previously reported (15,17). KR2 expression was induced in cells at an OD_{600} of 0.6 with IPTG (Carl Roth) in lysogeny broth medium supplemented with 5 μm all-*trans* retinal (Sigma Aldrich). Induced cells were grown for 3 h at 37°C and then harvested and disrupted using an EmulsiFlex-C3 Homogenizer (AVESTIN, Ottawa, ON, Canada). The membrane fraction was collected by ultracentrifugation at 45,000 rotations per minute for 1 h at 4°C, using a Type 45 Ti rotor (Beckman Coulter, Brea, CA). The membrane pellet was then resuspended in buffer containing 50 mM Tris-HCl (pH 8.0), 300 mM NaCl, 0.1 mM phenylmethylsulfonyl fluoride (PMSF), 1.5% n-dodecyl-D-maltoside (DDM) (GLYCON Biochemicals, Luckenwalde, Germany), and 0.3% cholesteryl hemisuccinate (CHS; Sigma Aldrich) and stirred overnight for solubilization. The insoluble fraction was removed by ultracentrifugation at 200,000 × *g* for 1 h at 4°C, and recombinant KR2 protein was purified by Ni-NTA affinity using the ÄKTAxpress protein purification system (GE Healthcare Life Sciences, Marlborough, MA), configured with a HisTrap HP Ni-NTA column. The collected protein fractions were concentrated in buffer containing 50 mM Tris-HCl (pH 8.0), 150 mM NaCl, 0.1 mM PMSF, 0.02% DDM, and 0.004% CHS.

To analyze the spectroscopic characteristics of purified KR2-WT and the R109Q mutant in variable ionic and pH conditions, different buffers were utilized. Steady-state absorption was measured at pH 8.0 (50 mM Tris-$C_6H_8O_7$), pH 9.0 (50 mM glycine-*N*-methyl-*D*-glucamine [NMG]), and pH 10.0 (50 mM glycine-NMG). The salt conditions were 150 mM NaCl, LiCl, or KCl. In the case of steady-state absorption measurements at pH 9.0, a salt concentration of 110 mM was used. Flash photolysis measurements were performed with 150 mM NaCl at pH 8.0 (50 mM Tris-HCl) and with 150 mM KCl at pH 10.0 (50 mM glycine-NMG). All buffer exchange was performed using PD-10 Desalting Columns, with Sephadex G-25 resin (GE Healthcare Life Sciences).

Ultraviolet-visible spectroscopy

Steady-state ultraviolet-visible absorption spectra were recorded using a Cary 300 spectrophotometer (Varian, Palo Alto, CA) at a spectral resolution of 1 nm and at room temperature (22°C). The LKS.60 Laser Flash Photolysis Spectrometer (Applied Photophysics, Leatherhead, UK), with modifications, was used to measure microsecond-to-second changes in multiwavelength data sets at a resolution of 0.4 nm. To excite the sample, the laser pulse was tuned to 530 nm using the MagicPrism Inline Tunable Optical Parametric Oscillator (Opotek, Carlsbad, CA), which was pumped via the third harmonic of a BrilliantB Nd:YAG laser (Quantel, Newbury,

UK). The laser energy was adjusted to 5 mJ/shot and a pulse duration of 10 ns, and changes in absorption were measured with a 150 W Xenon lamp (Osram, Munich, Germany). The transient spectra were recorded using an Andor iStar ICCD camera (DH734; Andor Technology, Belfast, UK), at 36 different time points between 1 μs and 1 s (five points per decade, isologarithmically). To ensure complete recovery of the dark state before the following recording, the sample was held in the dark for 30 s, and the resulting data sets were averaged over at least 10 cycles.

Primary data analysis was performed using MATLAB R2016b (The MathWorks, Natick, MA) to calculate difference spectra and reconstruct the three-dimensional spectra. Global analysis of the spectral data sets was performed with Glotaran 1.5.1 (Vrije Universiteit Amsterdam, Netherlands) (18). Singular value decomposition analysis of the data was used to determine the number of significant components needed to reconstruct the signal from the data sets, enabling noise reduction.

RESULTS

WT photocurrents in oocytes

We initially measured the photocurrents of KR2-WT in *Xenopus* oocytes and found that these were barely detectable. However, addition of the H^+/K^+-ATPase β-subunit fragment ("βHK") to the N-terminus improved the photocurrents substantially (Fig. S1, *B* and *C*), a strategy first established for bacteriorhodopsin (BR) (19). Therefore, unless otherwise stated, all measurements in *Xenopus* oocytes were performed with this $KR2_{\beta HK}$ construct (named KR2 in the following). KR2 photocurrents reached values up to 150 nA depending on the voltage, the extracellular pH value (pH_o), and the ionic conditions (Fig. 1 *B*; Fig. S5 *A*). The characteristic initial transient peak after light on is followed by stationary photocurrents (Fig. 1 *C*), and overall, these results for KR2-WT are consistent with earlier reports (13,15,17). We further found that photocurrents and pH_o dependence are unaffected by the replacement of extracellular NaCl with KCl (Fig. S5 *A*). In contrast, stationary photocurrent amplitudes are slightly reduced by replacement of extracellular sodium or potassium ions with NMG-Cl, LiCl, $MgCl_2$, or $CaCl_2$ (Figs. S5 *A* and S6 *C*). However, under all conditions, photocurrents were found to be positive, confirming the outward-directed pumping activity of KR2. Photocurrents of other sodium pumps, including those from *Nonlabens dokdonensis* (NdR2), *N. marinus* (NMR2), *Nonlabens* sp. YIK11, *Gillisia limnaea*, *Indibacter alkaliphilus*, and *Truepera radiovictrix* (TrNaR1 and TrNaR2) (12,20–27), were also measured with and without βHK-targeting, but in all cases, the currents remained poor compared to $KR2_{\beta HK}$ (Fig. S1, *A*, *B*, and *D*; alignment in Fig. S2).

Introduction of leak mutations into KR2

The counterion complex (also called the "active site") is composed of residues interacting directly or indirectly with the protonated Schiff base and the extracellular half channel. It is a critical region in light-driven proton pumps that enables active pumping at substantial electrochemical loads and prevents passive proton backflow during illumination (9). Therefore, we mutated corresponding positions of the counterion complex in KR2, as illustrated in Fig. 1 *D*, using the published KR2 crystal structure (Protein Data Bank [PDB]: 3X3C) solved at neutral pH (15).

In KR2, position D116 is predicted to act as the primary proton acceptor of the protonated Schiff base. However, D116 is protonated at low pH (12,15,28), consistent with the low activity of KR2 observed at pH_o 5.0 (Fig. S5 *A*). Indeed, the KR2-D116N mutant, which mimics the protonated state, showed no distinct stationary photocurrents (Fig. 1 *E*). Nevertheless, some diverse and highly pH_o-dependent transient photocurrents—reflecting charge movements within the protein—remained and reversed to inward at low pH_o. In addition, positions S70 and N112 are located in close proximity to D116 (Fig. 1 *D*), and both single mutants, S70A and N112D, showed reduced outward photocurrents with pronounced initial peak currents (Fig. 1, *B*, *F*, and *G*; Fig. S5, *B* and *C*).

Mutation of the second predicted counterion, D251 to N, resulted in only small transient photocurrents and a total loss of stationary photocurrents (Fig. 1 *H*). This outcome was unexpected because of the fact that the homologous mutation in the CsR proton pump (CsR-D211N) induces passive proton conductance (9). However, the conservative mutation, KR2-D251E, showed stationary inward photocurrents, indicating pump leakiness (Fig. 1, *B* and *I*), but with amplitudes smaller than 10 nA. Further, replacement of extracellular Na^+ with either K^+ or Li^+ led to changes in the reversal potential, indicating nonselective passive cation conductance in KR2-D251E (Fig. S5 *D*). Interestingly, KR2-L75K also displayed inward stationary photocurrents at negative membrane voltage (Fig. 1, *B* and *J*). This mutation was also encouraged by our earlier experiments in which the homologous mutation ($\triangleq$ CsR-Y57K, BR-Y57K) converted the proton pumps CsR and BR into outward rectifying proton channels (9). The strong pH_o dependency was conserved in KR2-L75K, but more negative reversal potentials were observed for all ionic conditions, indicating that ion leakiness is poor compared to D251E (Fig. S5 *E*).

Potassium selectivity in KR2-R109Q

Nearly all microbial rhodopsins contain a highly conserved arginine (e.g., KR2-R109, BR-R82, CsR-R83, ChR2-R120) in the extracellular half channel, near the counterion complex (Fig. 1 *D*; alignment in Fig. S2), with the exception of channelrhodopsins from the alga *Guillardia theta* (29,30) and inward H^+-pumping xenorhodopsins (31). Notably, previous reports have indicated that mutation of this conserved arginine in proton pumps also results in proton leakage at moderate electrochemical load with residual pump activity (9). Here, we mutated the conserved arginine

at position 109 in KR2 to generate KR2-R109Q. Our results suggest that this mutant is a passive potassium channel with unexpected properties, as described in the following.

Fig. 2 *A* shows representative photocurrent traces of KR2-R109Q at different extracellular cation conditions (all pH_o 10, with 100 mM NaCl, 100 mM KCl, or 100 mM LiCl). The cytoplasm of *X. laevis* oocytes contains ~5–10 mM Na^+ and 80–140 mM K^+ (32). With extracellular 100 mM NaCl, there exists an inward-directed chemical gradient for Na^+ and an outward-directed gradient for K^+. Therefore, the observed outward currents in Fig. 2 *A* (*left*) can be explained by either cation pump activity or passive transport of K^+ ions. Further, pronounced bidirectional stationary photocurrents were only observed in presence of extracellular KCl (100 mM in Fig. 2 *A*, *middle*). In this case, inward currents can only be explained by passive K^+ influx because the proton gradient was outward-directed (high pH_o). Additionally, passive proton transport is excluded because the reversal potentials are not affected by the pH gradient (E_{rev} in Fig. 2 *B*). Nevertheless, the current-voltage relationship for KR2-R109Q (Fig. 2 *B*) demonstrates that photocurrents are strongly promoted by alkaline pH_o, even more pronounced than in KR2-WT (illustrated in Fig. S6 *B* as the ratio pH_o 10/7.5, measured at 100 mM KCl). Lithium ions are also passively transported but with reduced efficiency because these are associated with smaller inward currents, despite the higher Li^+ gradient (Fig. 2 *A*, *right*).

We next performed a stepwise reduction of extracellular K^+ and observed changes of the reversal potential as expected for a passive K^+ conductance (Fig. 2, *C* and *D*). The theoretically expected reversal potentials for an ideal passive potassium channel are shown in Fig. 2 *D*. However, the experimentally recorded reversal potentials (Fig. 2 *D*) are more positive than the calculated values (Δ15 mV for K_o = 200 mM) indicating either small residual pump activity or a small passive conductance for Na^+. As support of small passive Na^+ conductance, tiny inward currents were observed in the presence of extracellular Na^+ already at pH_o 7.5, which disappeared after replacement of NaCl with NMG-Cl, $MgCl_2$, or $CaCl_2$ (Fig. S6, *D* and *E*). Contribution of chloride is unlikely because current-voltage relationships are unchanged after replacement of 100 mM NaCl with 100 mM Na-gluconate (Fig. S6 *E*). Interestingly, we observed that currents were reduced by more than half in a mixture of "50 mM NaCl and 50 mM KCl" compared with "50 mM KCl," suggesting that Na^+ inhibits K^+ conductance. Na^+ itself is not passively conducted in this mixture of Na^+/K^+ ions because the reversal potentials remained unaffected (Fig. S6 *F*).

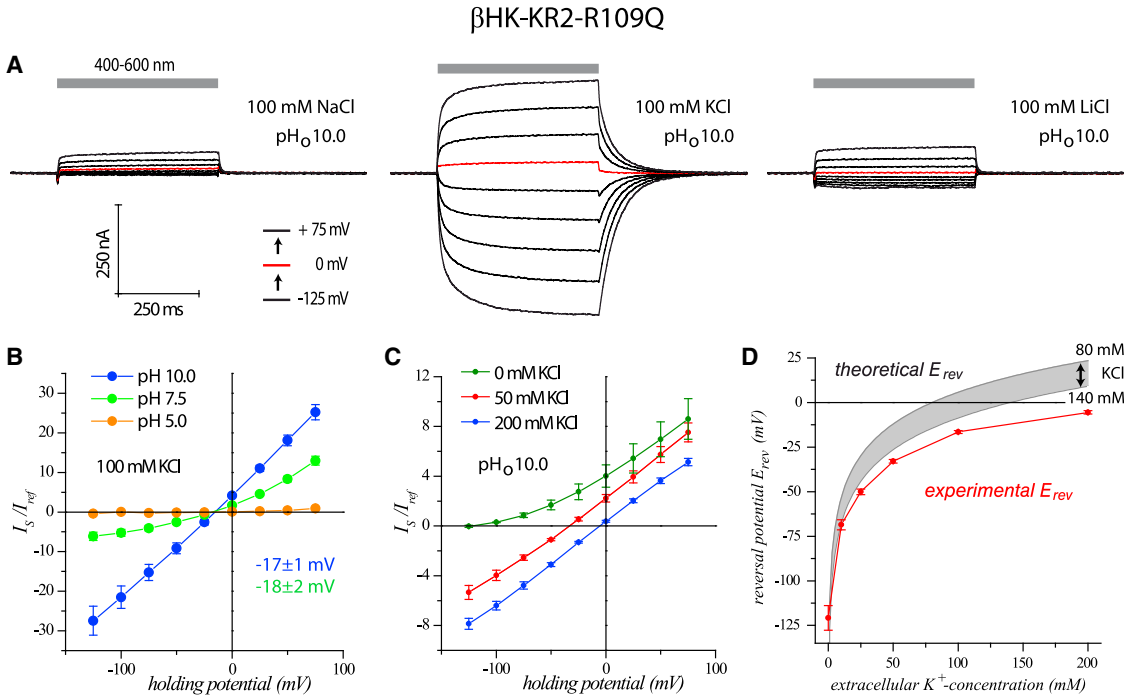

FIGURE 2 Analysis of the K^+-selective mutant, $KR2_{\beta HK}$-R109Q, in *X. laevis* oocytes. (*A*) Photocurrent traces from a single oocyte at different extracellular ion conditions are shown: 100 mM NaCl (*left*), KCl (*middle*), or LiCl (*right*), and holding potentials (in 25 mV steps; *red trace* indicates 0 mV). (*B*) A current-voltage plot at different extracellular pH values (all 100 mM KCl, normalized to buffer with 100 mM NaCl (pH_o 7.5) and 0 mV) is shown; pH_o 10/7.5/5.0 (n = 16/8/3). (*C*) A current-voltage plot of extracellular K^+ ion titration demonstrates that inward-directed photocurrents are carried by passive transport of K^+ ions (normalized to buffer with 100 mM KCl, pH_o 10.0, and 0 mV); 0/50/100 mM KCl (n = 4/4/5). (*D*) Comparison of the experimentally calculated reversal potentials with the theoretically expected reversal potentials for pure passive K^+ conductance is shown (calculated with intracellular K^+ concentrations of 80 and 140 mM); 0/10/25/50/100/200 mM KCl (n = 4/2/3/4/16/5). To see this figure in color, go online.

In addition, replacement of R109 with either alanine or asparagine (KR2-R109A and KR2-R109N, respectively) also resulted in pump leakiness but with reduced photocurrent amplitudes (Figs. S1 *C* and S6 *A*). For KR2-R109N in particular, the reversal potentials shifted to more positive values, and an extended passive conductance for Na^+ was observed (Fig. S5, *F–H*). These results indicate that position R109 is not only involved in preventing leakiness but also plays a role in ion selectivity itself.

We then investigated the importance of position KR2-R109 in other NaRs. In particular, both NdR2 and NMR2 displayed small, but sufficient, photocurrents of up to 50 nA in our initial screen (Figs. S1 *C* and S7, *A* and *B*). Notably, the mutated pumps (NdR2-R109Q and NMR2-R108Q) also showed cation leakiness and strong pH_o dependency but with ion selectivity that was distinct from KR2-R109Q. Unexpectedly, for the rhodopsin TrNaR2, bidirectional photocurrents were recorded with the WT protein (Fig. S7 *C*), and inward photocurrents disappeared after removal of extracellular sodium ions (Fig. S7 *D*). This indicates that TrNaR2 might have a natural leakiness for cations or is still a natural cation channel; however, further analysis of TrNaR2 was not possible because of the weak photocurrent amplitudes observed with this protein.

Voltage-clamp experiments in ND7/23-cells

We next performed voltage-clamp whole-cell analyses in ND7/23-cells, which allowed the control of intracellular buffer conditions. Because membrane targeting of $KR2_{\beta HK}$ is poor in ND7/23-cells, for these experiments, we used the well-targeted eKR2 construct instead (17). To ensure construct design had no effect on electrical properties, we compared $KR2_{\beta HK}$ and eKR2 in oocytes. Current-voltage relationships were similar with the exception that the K^+ conductance was reduced in eKR2-R109Q, with E_{rev} shifted from −17 to −31 mV (Fig. S8, *A–E*). In addition, inhibition of endogenous potassium channels with triethylamine (TEA, 20 mM), $BaCl_2$ (5 mM), and CsCl (5 mM) in the buffers (Fig. S4) was critical for observing photocurrents of eKR2-R109Q at high intra- and extracellular K^+ concentrations in ND7/23-cells.

The experiments in ND7/23-cells confirmed that the mutant eKR2-R109Q passively conducts potassium and lithium because inward currents were observed at low intracellular cation concentrations (1 mM NaCl, 1 mM KCl) and high extracellular K^+ or Li^+ concentrations (110 mM KCl or LiCl) (Fig. 3 *A*). Inward currents were reduced after increasing the intracellular K^+ concentration from 1 to 110 mM (see Fig. 3 *B*).

In addition, we conclude that eKR2-R109Q was still capable of pumping Na^+, and passive inward currents were only apparent if the intracellular Na^+ concentration was low. This conclusion is based on the following measurement (Fig. 3 *C*): only outward photocurrents were observed at each voltage and extracellular ion state at high intracellular Na^+ concentrations (110 mM NaCl, 1 mM KCl). Such residual pump activity is in line with the observed differences between the measured and calculated reversal potentials in oocytes (Fig. 2 *D*).

KR2-S70 is critical for sodium pump activity in R109Q

Within the hydrogen bonding network of the counterion complex, we identified KR2-S70 as a residue that may be critical for the residual Na^+ pumping activity still observed in KR2-R109Q. The single mutant, KR2-S70A, remained an outward-directed pump without any leakiness in oocytes (Fig. 1 *G*; Fig. S6 *A*). Combination of KR2-R109Q with the S70A substitution, however, led to strong passive transport for all tested cations, with the exception of protons (Fig. 4, *A–C*). Inward-directed photocurrent amplitudes of this double mutant were also tenfold larger than for KR2-WT, highlighting its pronounced channel-like behavior (Fig. S6 *A*), although pH_o dependence was further increased (Fig. 4 *C*; Fig. S6 *B*).

We also tested the double mutant, eKR2-S70A-R109Q, in ND7/23-cells and observed negative photocurrents at inward-directed electrochemical gradients (Fig. 4, *D* and *E*). Here, the possibility of a small residual pump activity cannot be excluded because of the fact that small outward currents were observed at a high inward-directed K^+ gradient, as shown in Fig. 4 *D* (extracellular: 110 mM KCl and 1 mM NaCl, intracellular: 0.1 mM NaCl and 0.1 mM KCl). Without a chemical gradient for Na^+, bidirectional photocurrents were observed, depending on the electrical gradient (Fig. 4 *F*, *top*). Further, in this double mutant, Na^+ transport outperformed K^+ transport, as indicated by asymmetric Na^+ and K^+ distributions (Fig. 4 *F*, *bottom*). This can be explained by the residual pumping or higher passive conductance of Na^+.

Reduction of the pH_o dependence

Previous results (15) combined with our own observations indicate a strong pH_o dependence of KR2 photocurrents at low internal Na^+. Conversely, intracellular pH appears to exert only a minor influence on KR2 photocurrents (17). Interestingly, we found that pH_o dependence is further increased for KR2 constructs containing the leak mutations, particularly in the double mutant KR2-S70A-R109Q (Fig. 4 *B*; Fig. S6 *B*), which limits their potential for use in optogenetic applications in neurons. These observations suggest that one or more charged residues are accessible from the extracellular side and reversibly protonated. Kato et al. reported (15) that at neutral pH, the KR2 structure contains the deprotonated D116 oriented toward the Schiff base and without a water molecule between D251 and R109 (as

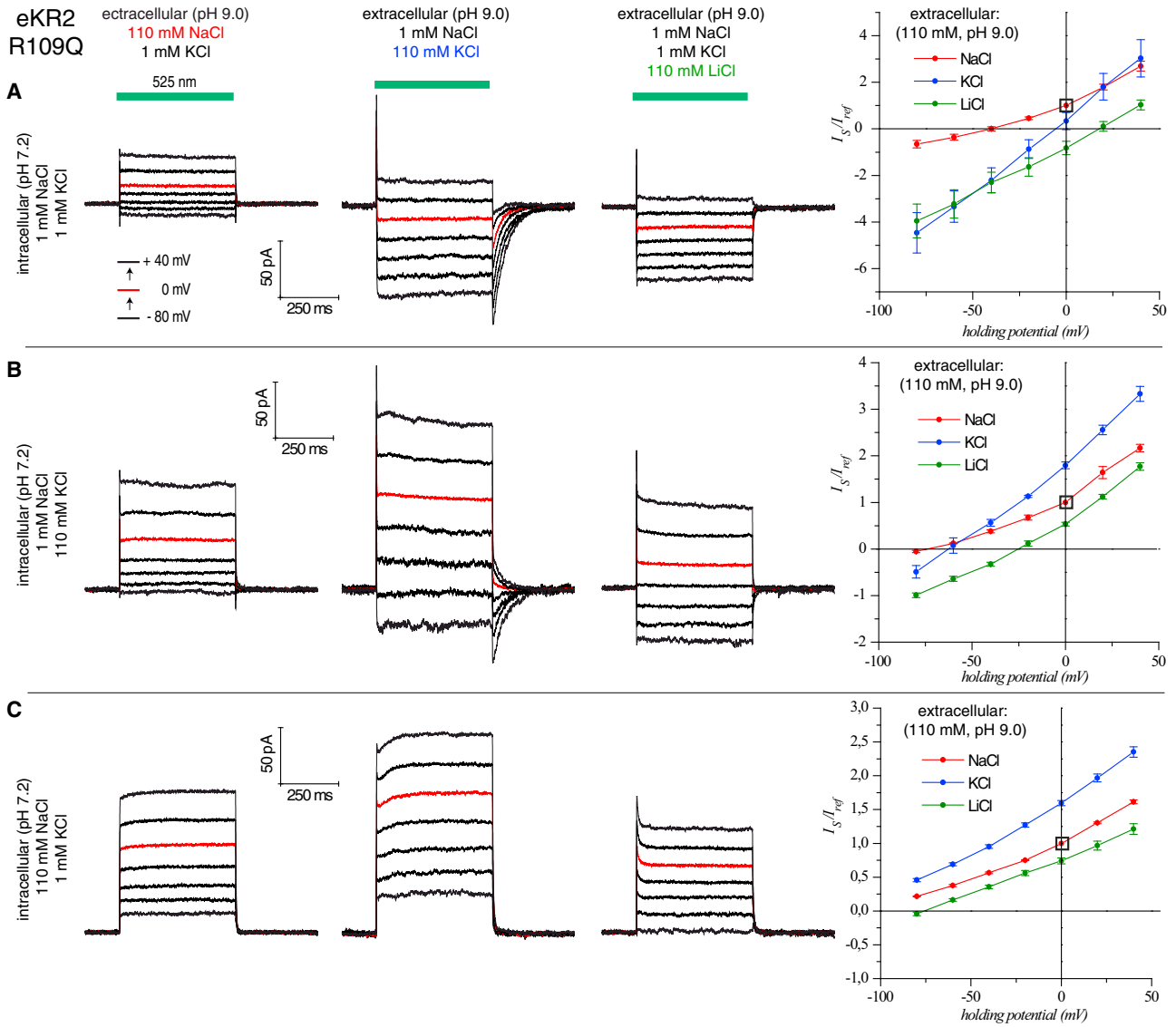

FIGURE 3 Electrophysiological analysis of eKR2-R109Q with controlled intracellular ion conditions in ND7/23-cells and, therefore, with defined cation gradients. The extracellular buffers were varied, whereas the intracellular conditions remained constant during the patch. For all three intracellular conditions tested (*A–C*), the current curves of a single cell (holding potentials in 20 mV steps; *red curve* shows 0 mV) and the corresponding current-voltage diagrams from several measurements are shown (normalized to 110 mM NaCl (pH_o 9.0) and 0 mV). (*A*) Intracellular: 1 mM Na^+ and 110 mM K^+. Extracellular: 110 mM NaCl, KCl, or LiCl (n = 4/4/4). (*B*) Intracellular: 1 mM Na^+ and 110 mM K^+. Extracellular: 110 mM NaCl, KCl, or LiCl (n = 6/5/5). (*C*) Intracellular: 110 mM Na^+ and 1 mM K^+. Extracellular: 110 mM NaCl, KCl, or LiCl (n = 6/5/5). To see this figure in color, go online.

shown in Fig. 1 *D*). In the acidic structure, D116 is protonated and reoriented toward S70. Clearly, this protonated state is nonfunctional and exhibits no stationary photocurrents. However, beyond the deprotonation of D116, other residues also seem to be important for the pH dependence of KR2 function because the transient photocurrents of KR2-D116N (Fig. 1 *E*) were found to be pH_o dependent (note that the KR2-R109Q-D116N/A mutants were nonfunctional).

Based on these considerations, various double mutant combinations with R109Q were tested to determine whether they can reduce pH_o dependence (see Fig. S10). Of these, only the double mutant KR2-R109Q-D251N exhibited reduced pH_o dependence between pH_o 10 and pH_o 7.5 (Fig. S6, *A* and *B*), suggesting that D251 is involved. However, this mutant also showed a restoration of ion-pumping activity, as indicated by the negative shift of E_{rev} (Fig. S5 *I*). These data seem to be inconsistent with results from the single mutant, D251N (Fig. 1 *H*), which showed neither active nor passive photocurrents and only a transient charge movement upon light on, whereas the combination with R109Q rescued functionality.

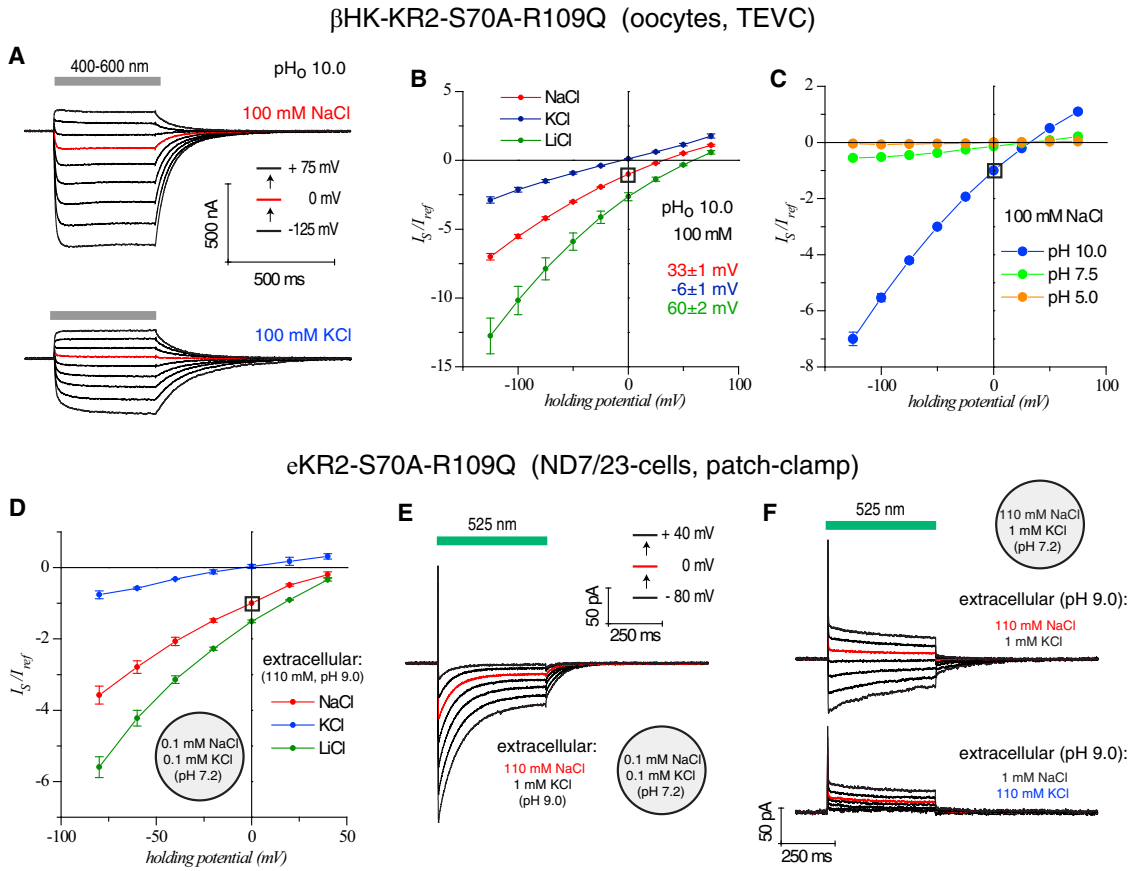

FIGURE 4 Electrophysiological investigation of the Na^+-conducting channel-like double mutant, KR2-S70A-R109Q, in oocytes (βHK) and ND7/23-cells (eKR2). (*A*) Photocurrent traces from a single oocyte at 100 mM NaCl or 100 mM KCl (both extracellular) and holding potentials (in 25 mV steps; *red trace* indicates 0 mV) are shown. (*B* and *C*) Current-voltage plots of the double mutant, KR2-S70A-R109Q, at different extracellular ion and pH conditions, measured in oocytes, are shown (normalized to 100 mM NaCl (pH_o 10.0) and 0 mV); 110 mM NaCl/KCl/LiCl (n = 15/10/7), pH_o 10/7.5/5.0 (n = 15/6/4). (*D*) Current-voltage plot of stationary photocurrents from patch-clamp measurements with strong inward-directed chemical gradients for Na^+, K^+, or Li^+ are shown (normalized to 110 mM NaCl (pH_o 9.0) and 0 mV); 110 mM NaCl/KCl/LiCl (n = 2/2/2). (*E*) Photocurrent traces from a single ND7/23-cell with a high inward-directed Na^+ gradient are shown (in 20 mV steps; *red trace* indicates 0 mV). (*F*) Photocurrents from a single ND7/23-cell with a no-chemical gradient (*upper traces*) or with competition between an inward-directed Na^+ and an outward-directed K^+ gradient (*bottom*) are shown. To see this figure in color, go online.

Functional expression in *E. coli* and characterization of purified KR2-R109Q

Lastly, we expressed KR2-R109Q in *E. coli* and found that illumination of cells expressing this protein did not promote substantial pH changes in the cell suspension but did lead to alkalization after addition of the protonophore, CCCP, in 100 mM NaCl (Fig. 5 *A*). This can be interpreted as residual outward-directed Na^+ pumping at low membrane voltage (Fig. S9 *B*). We did not observe any light-induced pH changes for cell suspensions of KR2-R109A, R109N, or S70A-R109Q (Fig. S9).

We further found that the absorption maximum of recombinant KR2-R109Q was 16–21 nm red-shifted at pH 8.0 compared to KR2-WT, but this shift is reduced at pH 10 (Fig. 5 *B*; Fig. S8, *F–H*). These data suggest that the R109 substitution increases the pK_a of D251 or D116, causing protonation at neutral pH and deprotonation only at high pH. In addition, time-resolved flash photolysis experiments revealed that KR2-R109Q shows a prolonged K-state decay, without an obvious L- and M-intermediate (Fig. 5, *C* and *D*). The O-intermediate was also less prominent because of protonation of D251 and was only detectable at alkaline pH when D251 deprotonates. Overall, the spectral data revealed that pH has a strong impact on the KR2-R109Q photocycle and its kinetics, which is consistent with our electrical recordings.

DISCUSSION

In this study, we used mutagenesis, electrophysiology analysis, and spectroscopy to investigate the potential for conversion of NaRs, such as KR2, into passive cation channels. Our results reveal that cation leakiness can be introduced into these NaRs, and moreover, even

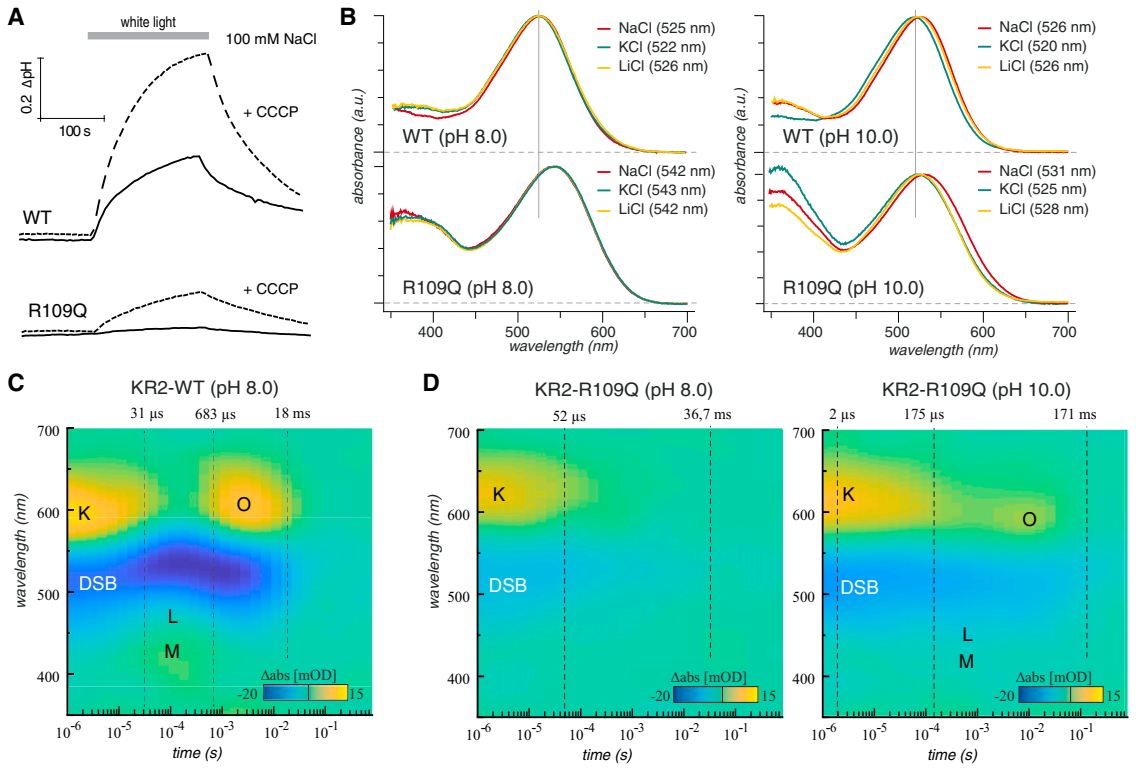

FIGURE 5 Expression and spectroscopic investigation of KR2-WT and KR2-R109Q in *E. coli*. (*A*) Light-induced pH changes in suspensions of *E. coli* cells expressing KR2-WT or KR2-R109Q (in 100 mM NaCl) are shown. (*B*) Absorption spectra of purified KR2 (*upper panel*) and KR2-R109Q (*lower panel*) recorded at pH 8.0 (*left*) and pH 10.0 (*right*) and variable ionic conditions are shown: 150 mM NaCl (*red*), 150 mM KCl (*green*), or 150 mM LiCl (*yellow*). (*C* and *D*) Reconstructed absorption difference surface plots are shown from flash photolysis measurements on purified recombinant (*C*) KR2 (150 mM NaCl) and (*D*) KR2-R109Q (150 mM NaCl (pH 8) and 150 mM KCl (pH 10)). The spectral data were globally fitted, and the resulting photointermediate decay τ values are indicated in the surface plots. To see this figure in color, go online.

discrimination between Na^+ and K^+ ions is possible. We further analyzed the KR2-R109Q mutant, which shows passive and selective conductance for potassium ions, in more detail in oocytes and ND7/23-cells. Despite its passive K^+ conductance, KR2-R109Q still functions as an active outward-directed Na^+ pump if intracellular Na^+ ions are available and the counterion D116 is deprotonated in the dark state.

Residual pumping in KR2-R109Q is supported by the following observations: first, outward-directed photocurrents were detected against an inward-directed electrochemical gradient for Na^+ in TEVC experiments in oocytes (Fig. 2 *A*, *left*). Second, only outward photocurrents were observed in whole-cell voltage-clamp measurements with high intracellular Na^+ concentrations, as well as in those with a symmetrical chemical gradient for Na^+ (Fig. 3 *C*). Finally, a slight alkalization of the extracellular medium (passive H^+ influx facilitated by CCCP) was detected upon illumination of *E. coli* suspensions expressing KR2-R109Q in 100 mM NaCl (Fig. 5 *A*). In all cases, when the intracellular Na^+ concentration is lower than ~5–10 mM and extracellular K^+ is high (110 mM), the KR2-R109Q mutant shows passive inward leakage for cations (preferentially K^+) in both oocytes and ND7/23-cells (Figs. 2 and 3).

Moreover, as previously noted for KR2-WT in ND7/23-cells and suggested by the pH assay in *E. coli*, our measurements indicate a strong dependency of photocurrent amplitudes on extracellular pH_o for all tested NaRs and their mutants under physiological, i.e., low, intracellular sodium concentrations (16,17). Critically, an enhanced understanding of this characteristic feature of NaRs will be important for enabling the use of passive conducting mutants in optogenetic applications. Here, it was possible to reduce the pH_o dependency of KR2-R109Q in the double mutant, KR2-R109Q-D251N, but only with a concomitant loss of passive conductance (Figs. S5 *I* and S6, *A* and *B*).

Based on our results, we conclude that leak mutations R109Q and L75K increase the pK_a value of the aspartate D251 and that therefore alkaline pH values are necessary for maintenance of the deprotonated states. This is supported by the observation that the absorption spectrum maximum of KR2-R109Q is red-shifted at pH 8 (Fig. 5 *B*). For the proton pump BR, it is well known that residue R82 influences the protonation states of the counterion complex, as well as for other residues in the extracellular half channel (33,34). We propose a similar importance of R109 in stabilization of pK_a values in

NaRs, and we further suggest that this residue serves a gate function for central restriction, which separates the cavity of the Schiff base from the ion-release cavity (16). It is likely that this restriction prevents the passive backflow of cations during the photocycle. Lastly, we hypothesize that pH_o dependency arises because of the combination of the protonation states of D116 and D251 and their pH-dependent interactions with other residues of the counterion complex in both dark state and during the photocycle. Thus, this obstacle is not easy to overcome for development of a light-gated K^+ channel that is fully functional at neutral pH_o.

CONCLUSIONS

There continues to be a demand for the development of light-gated selective K^+ channels, particularly for neuronal silencing, using light of moderate-to-low intensities. A number of attempts have been made to generate such channels (35–41), but all available constructs developed to date have specific drawbacks, such as weak expression, poor membrane targeting, slow kinetics, need for incubation with chemical compounds, and significant dark activity. Consistent with these limitations, all attempts to introduce high K^+ selectivity directly in channelrhodopsins have also failed (42,43). Here, our results show that ion selectivity for K^+ over Na^+ for passive transport can be introduced into a microbial rhodopsin starting from the Na^+-pump KR2, but more work will be necessary to generate a channel that functions at neutral pH.

SUPPORTING MATERIAL

Supporting Material can be found online at https://doi.org/10.1016/j.bpj.2019.04.001.

AUTHOR CONTRIBUTIONS

A.V. and P.H. designed the study. A.V. designed and measured NaR constructs and their mutants in oocytes and ND7/23-cells and performed pH measurements with *E. coli* cells. A.S. cloned and purified the protein from *E. coli* and performed spectroscopic experiments. C.G. provided the targeting variant for mammalian cells, made early recordings in ND7/23 cells, and supported the *E. coli* measurements. F.H. and M.A.M. supported measurements in oocytes. A.V. wrote the manuscript, with support from P.H., C.G., and A.S. All authors approved the final version of the article.

ACKNOWLEDGMENTS

We thank Altina Klein, Maila Reh, and Tharsana Thamalingam for technical assistance. We also thank Roman Fudim for helpful discussions.

This work was supported by the Deutsche Forschungsgemeinschaft (SPP 1926, SFB 1078, UniCat), the Gottfried Wilhelm Leibniz-Preis, and the European Union's Horizon 2020 (Stardust) program. P.H. is senior professor for neuroscience, supported by the Hertie Foundation.

REFERENCES

1. Ernst, O. P., D. T. Lodowski, …, H. Kandori. 2014. Microbial and animal rhodopsins: structures, functions, and molecular mechanisms. *Chem. Rev.* 114:126–163.
2. Hochbaum, D. R., Y. Zhao, …, A. E. Cohen. 2014. All-optical electrophysiology in mammalian neurons using engineered microbial rhodopsins. *Nat. Methods.* 11:825–833.
3. Wiegert, J. S., M. Mahn, …, O. Yizhar. 2017. Silencing neurons: tools, applications, and experimental constraints. *Neuron.* 95:504–529.
4. Rost, B. R., F. Schneider-Warme, …, P. Hegemann. 2017. Optogenetic tools for subcellular applications in neuroscience. *Neuron.* 96:572–603.
5. Gadsby, D. C. 2009. Ion channels versus ion pumps: the principal difference, in principle. *Nat. Rev. Mol. Cell Biol.* 10:344–352.
6. Hegemann, P., M. Fuhrmann, and S. Kateriya. 2001. Algal sensory photoreceptors. *J. Phycol.* 37:668–676.
7. Nagel, G., D. Ollig, …, P. Hegemann. 2002. Channelrhodopsin-1: a light-gated proton channel in green algae. *Science.* 296:2395–2398.
8. Nagel, G., T. Szellas, …, E. Bamberg. 2003. Channelrhodopsin-2, a directly light-gated cation-selective membrane channel. *Proc. Natl. Acad. Sci. USA.* 100:13940–13945.
9. Vogt, A., Y. Guo, …, P. Hegemann. 2015. Conversion of a light-driven proton pump into a light-gated ion channel. *Sci. Rep.* 5:16450.
10. Inoue, K., T. Tsukamoto, …, Y. Sudo. 2015. Converting a light-driven proton pump into a light-gated proton channel. *J. Am. Chem. Soc.* 137:3291–3299.
11. Takayama, R., A. Kaneko, …, Y. Sudo. 2018. Production of a light-gated proton channel by replacing the retinal chromophore with its synthetic vinylene derivative. *J. Phys. Chem. Lett.* 9:2857–2862.
12. Inoue, K., H. Ono, …, H. Kandori. 2013. A light-driven sodium ion pump in marine bacteria. *Nat. Commun.* 4:1678.
13. Tsunoda, S. P., M. Prigge, …, H. Kandori. 2017. Functional characterization of sodium-pumping rhodopsins with different pumping properties. *PLoS One.* 12:e0179232.
14. Kandori, H., K. Inoue, and S. P. Tsunoda. 2018. Light-driven sodium-pumping rhodopsin: a new concept of active transport. *Chem. Rev.* 118:10646–10658.
15. Kato, H. E., K. Inoue, …, O. Nureki. 2015. Structural basis for Na(+) transport mechanism by a light-driven Na(+) pump. *Nature.* 521:48–53.
16. Gushchin, I., V. Shevchenko, …, V. Gordeliy. 2015. Crystal structure of a light-driven sodium pump. *Nat. Struct. Mol. Biol.* 22:390–395.
17. Grimm, C., A. Silapetere, …, P. Hegemann. 2018. Electrical properties, substrate specificity and optogenetic potential of the engineered light-driven sodium pump eKR2. *Sci. Rep.* 8:9316.
18. Snellenburg, J. J., S. Laptenok, …, I. H. M. van Stokkum. 2012. Glotaran: a Java-based graphical user interface for the R package TIMP. *J. Stat. Softw.* 49:22.
19. Geibel, S., T. Friedrich, …, E. Bamberg. 2001. The voltage-dependent proton pumping in bacteriorhodopsin is characterized by optoelectric behavior. *Biophys. J.* 81:2059–2068.
20. Ivanova, N., C. Rohde, …, A. Lapidus. 2011. Complete genome sequence of Truepera radiovictrix type strain (RQ-24). *Stand. Genomic Sci.* 4:91–99.
21. Li, H., O. A. Sineshchekov, …, J. L. Spudich. 2015. In vitro demonstration of dual light-driven Na^+/H^+ pumping by a microbial rhodopsin. *Biophys. J.* 109:1446–1453.
22. Balashov, S. P., E. S. Imasheva, …, J. K. Lanyi. 2014. Light-driven Na(+) pump from Gillisia limnaea: a high-affinity Na(+) binding site is formed transiently in the photocycle. *Biochemistry.* 53:7549–7561.
23. Kwon, Y. M., S. Y. Kim, …, S. J. Kim. 2016. Diversity and functional analysis of light-driven pumping rhodopsins in marine Flavobacteria. *MicrobiologyOpen.* 5:212–223.

24. Yoshizawa, S., Y. Kumagai, …, K. Kogure. 2014. Functional characterization of flavobacteria rhodopsins reveals a unique class of light-driven chloride pump in bacteria. *Proc. Natl. Acad. Sci. USA.* 111:6732–6737.

25. Kwon, S. K., B. K. Kim, …, J. F. Kim. 2013. Genomic makeup of the marine flavobacterium Nonlabens (Donghaeana) dokdonensis and identification of a novel class of rhodopsins. *Genome Biol. Evol.* 5:187–199.

26. Yi, H., and J. Chun. 2012. Unification of the genera Nonlabens, Persicivirga, Sandarakinotalea and Stenothermobacter into a single emended genus, Nonlabens, and description of Nonlabens agnitus sp. nov. *Syst. Appl. Microbiol.* 35:150–155.

27. Yoon, J. H., S. J. Kang, …, T. K. Oh. 2012. Reclassification of the three species of the genus Krokinobacter into the genus Dokdonia as Dokdonia genika comb. nov., Dokdonia diaphoros comb. nov. and Dokdonia eikasta comb. nov., and emended description of the genus Dokdonia Yoon et al. 2005. *Int. J. Syst. Evol. Microbiol.* 62:1896–1901.

28. Shigeta, A., S. Ito, …, I. Kawamura. 2017. Solid-state nuclear magnetic resonance structural study of the retinal-binding pocket in sodium ion pump rhodopsin. *Biochemistry.* 56:543–550.

29. Govorunova, E. G., O. A. Sineshchekov, and J. L. Spudich. 2016. Structurally distinct cation channelrhodopsins from cryptophyte algae. *Biophys. J.* 110:2302–2304.

30. Yamauchi, Y., M. Konno, …, H. Kandori. 2017. Molecular properties of a DTD channelrhodopsin from Guillardia theta. *Biophys. Physicobiol.* 14:57–66.

31. Shevchenko, V., T. Mager, …, V. Gordeliy. 2017. Inward H^+ pump xenorhodopsin: mechanism and alternative optogenetic approach. *Sci. Adv.* 3:e1603187.

32. Sobczak, K., N. Bangel-Ruland, …, W. M. Weber. 2010. Endogenous transport systems in the Xenopus laevis oocyte plasma membrane. *Methods.* 51:183–189.

33. Otto, H., T. Marti, …, M. P. Heyn. 1990. Substitution of amino acids Asp-85, Asp-212, and Arg-82 in bacteriorhodopsin affects the proton release phase of the pump and the pK of the Schiff base. *Proc. Natl. Acad. Sci. USA.* 87:1018–1022.

34. Subramaniam, S., T. Marti, and H. G. Khorana. 1990. Protonation state of Asp (Glu)-85 regulates the purple-to-blue transition in bacteriorhodopsin mutants Arg-82——Ala and Asp-85——Glu: the blue form is inactive in proton translocation. *Proc. Natl. Acad. Sci. USA.* 87:1013–1017.

35. Banghart, M., K. Borges, …, R. H. Kramer. 2004. Light-activated ion channels for remote control of neuronal firing. *Nat. Neurosci.* 7:1381–1386.

36. Janovjak, H., S. Szobota, …, E. Y. Isacoff. 2010. A light-gated, potassium-selective glutamate receptor for the optical inhibition of neuronal firing. *Nat. Neurosci.* 13:1027–1032.

37. Fortin, D. L., T. W. Dunn, …, R. H. Kramer. 2011. Optogenetic photochemical control of designer K+ channels in mammalian neurons. *J. Neurophysiol.* 106:488–496.

38. Caro, L. N., C. J. Moreau, …, M. Vivaudou. 2012. Engineering of an artificial light-modulated potassium channel. *PLoS One.* 7:e43766.

39. Kang, J. Y., D. Kawaguchi, …, L. Wang. 2013. In vivo expression of a light-activatable potassium channel using unnatural amino acids. *Neuron.* 80:358–370.

40. Cosentino, C., L. Alberio, …, A. Moroni. 2015. Optogenetics. Engineering of a light-gated potassium channel. *Science.* 348:707–710.

41. Bernal Sierra, Y. A., B. R. Rost, …, D. Schmitz. 2018. Potassium channel-based optogenetic silencing. *Nat. Commun.* 9:4611.

42. Plazzo, A. P., N. De Franceschi, …, M. Mongillo. 2012. Bioinformatic and mutational analysis of channelrhodopsin-2 protein cation-conducting pathway. *J. Biol. Chem.* 287:4818–4825.

43. Kato, H. E., F. Zhang, …, O. Nureki. 2012. Crystal structure of the channelrhodopsin light-gated cation channel. *Nature.* 482:369–374.

Biophysical Journal, Volume *116*

Supplemental Information

Engineered Passive Potassium Conductance in the KR2 Sodium Pump

Arend Vogt, Arita Silapetere, Christiane Grimm, Florian Heiser, Maximiliano Ancina Möller, and Peter Hegemann

Supplementary Figure 1

A

abbreviation	organism	protein ID	type (habitat)	literature (cited in the main text)
KR2	*Dokdonia eikasta* (basonym: *Krokinobacter eikastus*)	N0DKS8	flavobacterium (seawater)	Yoon et al. 2012 Inoue et al. 2013
NdR2 (NQRh)	*Nonlabens dokdonensis* (basonym: *Donghaeana dokdonensis)*	L7W3L9	flavobacterium (seawater)	Yi et al. 2012 Kwon et al. 2013
NMR2	*Nonlabens marinus*	W8VZ79	flavobacterium (seawater)	Yoshizawa et al. 2014
YIK11	*Nonlabens sp.YIK11*	X2G242	flavobacterium (seawater)	Kwon et al. 2016
GLR	*Gillisia limnaea*	H2BW50	flavobacterium (antarctic lake)	Balashov et al. 2014
IAR	*Indibacter alkaliphilus*	S2D3K4	(non-flavo) bacterium (halo alkaline lake)	Li et al. 2015
TrNaR1	*Truepera radiovictrix*	D7CSE2	(non-flavo) bacterium (hot alkaline spring)	Ivanova et al. 2011
TrNaR2		D7CW88		

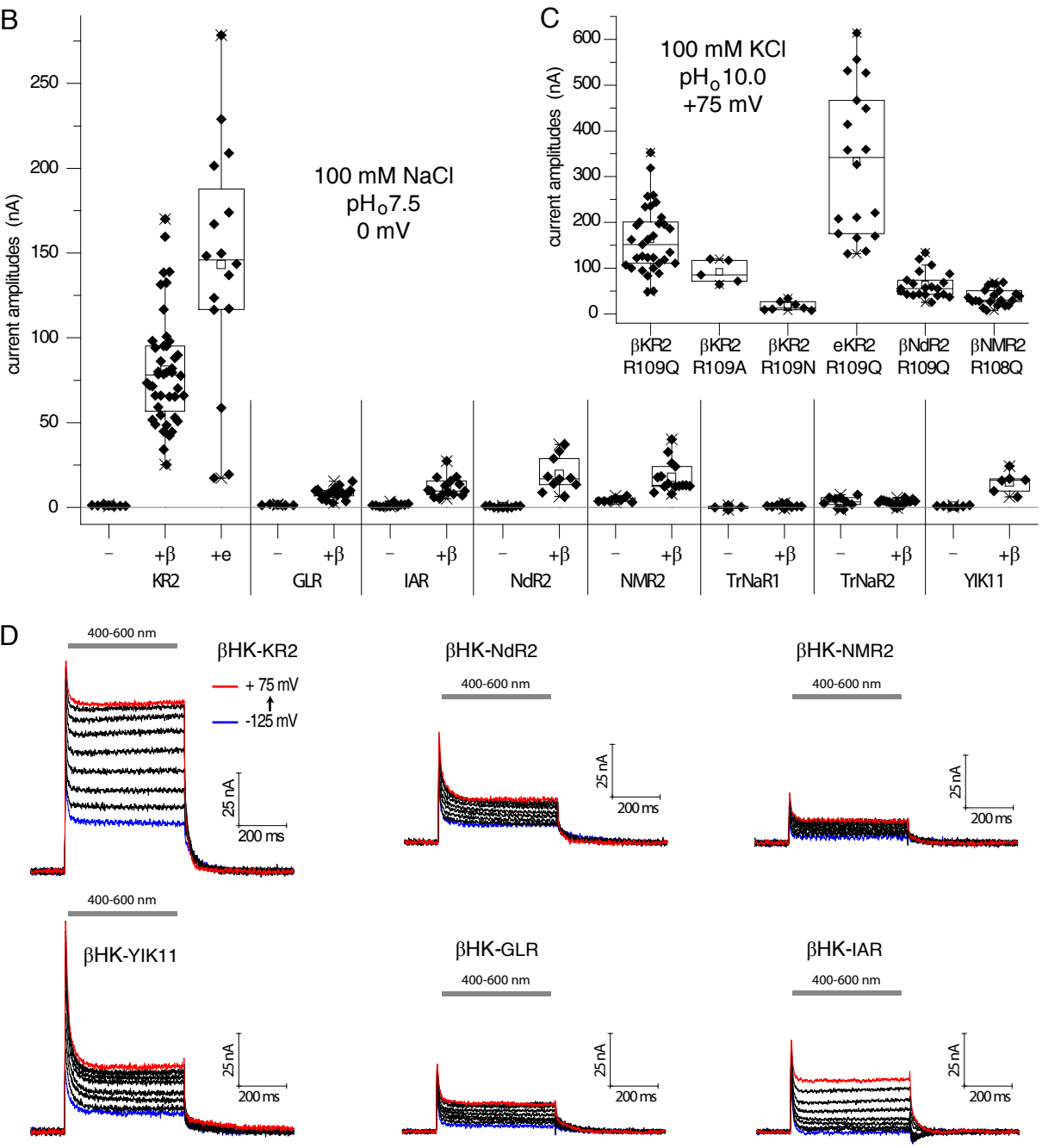

Supplementary Figure 1: Comparison of light-driven Na+ pumps from different organisms in oocytes. (*A*) List of NaRs tested in this study, with their origin and protein ID; references are provided in the main article. (*B-C*) Comparison of absolute stationary photocurrent amplitudes, shown as box-chart diagrams. Detectable photocurrents were only observed after addition of the "βHK"-targeting sequence (the eKR2 targeting design was only tested for KR2). (*C*) Stationary photocurrent amplitudes of the various R109X mutants are shown. In addition to KR2, only NdR2$_{\beta HK}$ and NMR2$_{\beta HK}$ provided sufficient photocurrents for testing the effect of the R109Q mutation (R108 in NMR2). (*D*) Photocurrent traces of various NaRs (all with "βHK") in buffer containing 100 mM NaCl, pH$_o$ 7.5. The IAR rhodopsin was remarkable in that produced showed negative peak-shaped photocurrents at negative holding potentials.

Supplementary Figure 2:

Multiple sequence alinment of NaRs and proton pumps

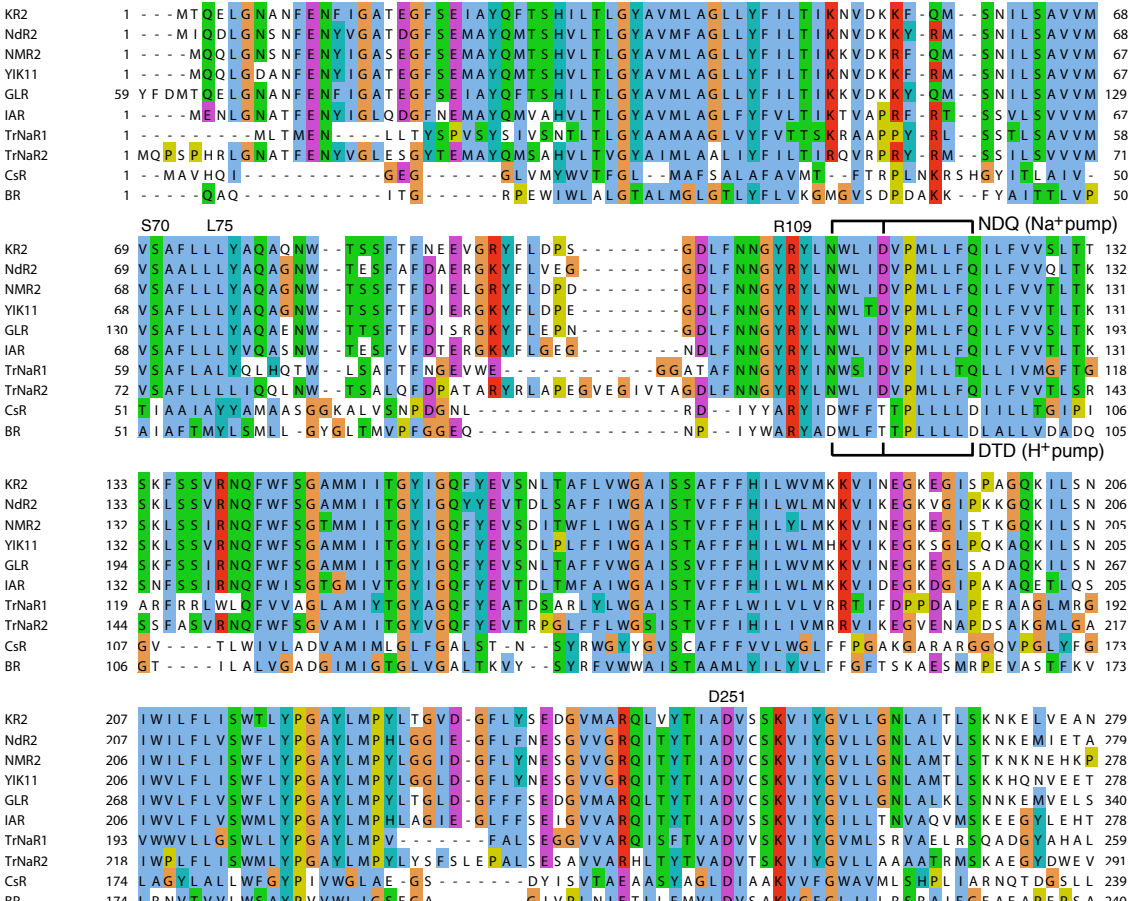

Supplementary Figure 3:

Nucleotide sequence of all tested KR2-constructs

KR2 (oocytes):

ATGACTCAGGAGCTGGGGAACGCTAATTTTGAGAACTTCATTGGAGCCACCGAGGGGTTTTCAGAGATCGCCTATCAGTTTACATCACACATTCTGACTCTGGGATATGCAGTCATGCTGGCCGGCCTGCTGTA
CTTTATCCTGACCATTAAGAACGTGGACAAGAAATTCCAGATGAGTAATATCCTGAGCGCCGTGGTCATGGTGAGCGCCTTCCTGCTGCTGTATGCCCAGGCTCAGAACTGGACTAGCTCCTTTACCTTCAATG
AGGAAGTGGGCCGGTACTTTCTGGACCCAAGTGGCGATCTGTTCAACAATGGGTACAGATATCTGAACTGGCTGATTGATGTGCCCATGCTGCTGTTTCAGATCCTGTTCGTGGTCAGCCTGACCACATCCAAA
TTCTCTAGTGTGAGGAACCAGTTTTGGTTCTCAGGCGCTATGATGATCATTACCGGCTATATTGGGCAGTTTTACGAGGTCAGCAATCTGACAGCATTCCTGGTGTGGGGGGCTATTTCAAGCGCATTCTTTTTC
CATATCCTGTGGGTCATGAAGAAAGTCATCAACGAGGGAAAGGAAGGCATTTCTCCCGCCGGACAGAAAATCCTGAGTAATATCTGGATTCTGTTTCTGATCTCCTGGACACTGTACCCCGGGGCTTATCTGAT
GCCTTACCTGACTGGGGTGGACGGATTCCTGTATTCTGAAGATGGAGTCATGGCACGGCAGCTGGTGTATACAATTGCCGACGTGTCCTCTAAGGTCATCTACGGGGTGCTGCTGGGCAATCTGGCAATTACC
CTGTCAAAAAACAAGGAACTGGTGGAGGCAAATAGCCCGCGGTGA

βHK-KR2 (oocytes):

ATGGCAGCCCTGCAGGAGAAGAAGTCATGCAGCCAGCGCATGGCCGAATTCCGGCAATACTGTTGGAACCCGGACACTGGGCAGATGCTGGGCCGCACCCCAGCCCGGTGGGTGTGGATCAGCCTGTACTA
TGCAGCTTTCTACGTGGTCATGACTGGGCTCTTTGCCTTGTGCATCTATGTGCTGATGCAGACCATTGATCCCTACACCCCCGACTACCAGGACCAGTTAAAGTCACCGGGGGGTAACCTTGAGACCGGATGTGT
ATGGGGAAAGAGGGCTGCAGATTTCCTACAACATCTCTGAAAACAGCTCTACTCAGGAGCTGGGGAACGCTAATTTTGAGAACTTCATTGGAGCCACCGAGGGGTTTTCAGAGATCGCCTATCAGTTTACATC
ACACATTCTGACTCTGGGATATGCAGTCATGCTGGCCGGCCTGCTGTACTTTATCCTGACCATTAAGAACGTGGACAAGAAATTCCAGATGAGTAATATCCTGAGCGCCGTGGTCATGGTGAGCGCCTTCCTGC
TGCTGTATGCCCAGGCTCAGAACTGGACTAGCTCCTTTACCTTCAATGAGGAAGTGGGCCGGTACTTTCTGGACCCAAGTGGCGATCTGTTCAACAATGGGTACAGATATCTGAACTGGCTGATTGATGTGCCC
ATGCTGCTGTTTCAGATCCTGTTCGTGGTCAGCCTGACCACATCCAAATTCTCTAGTGTGAGGAACCAGTTTTGGTTCTCAGGCGCTATGATGATCATTACCGGCTATATTGGGCAGTTTTACGAGGTCAGCAAT
CTGACAGCATTCCTGGTGTGGGGGGCTATTTCAAGCGCATTCTTTTTCCATATCCTGTGGGTCATGAAGAAAGTCATCAACGAGGGAAAGGAAGGCATTTCTCCCGCCGGACAGAAAATCCTGAGTAATATCT
GGATTCTGTTTCTGATCTCCTGGACACTGTACCCCGGGGCTTATCTGATGCCTTACCTGACTGGGGTGGACGGATTCCTGTATTCTGAAGATGGAGTCATGGCACGGCAGCTGGTGTATACAATTGCCGACGTG
TCCTCTAAGGTCATCTACGGGGTGCTGCTGGGCAATCTGGCAATTACCCTGTCAAAAAACAAGGAACTGGTGGAGGCAAATAGCCCGCGGTGA

eKR2 = C2C1-KR2-TS-eYFP-ER (oocytes):

ATGGACTATGGGGGAGCACTGTCCGCCGTCGGGCTGTTTCAGACTTCCTACACCCTGGAGAACAACGGGAGCGTCATTTGCATTCCTAACAATGGCCAGTGCTTCTGTCTGGCCTGGCTGAAGAGCAACGGGA
CCCAGGAACTGGGCAATGCCAACTTTGAGAATTTCATCGGCGCCACCGAGGGCTTTAGCGAGATCGCCTATCAGTTCACCTCCCACATCCTGACACTGGGCTATGCCGTGATGCTGGCCGGCCTGCTGTACTTT
ATCCTGACAATCAAGAACGTGGACAAGAAGTTCCAGATGTCTAATATCCTGAGCGCCGTGGTCATGGTGAGCGCCTTCCTGCTGCTGTATGCCCAGGCCCAGAACTGGACCAGCTCCTTTACATTCAATGAGG
AAGTGGGCAGGTACTTTCTGGACCCATCCGGCGATCTGTTCAACAATGGCTACAGATATCTGAACTGGCTGATCGATGTGCCCATGCTGCTGTTTCAGATCCTGTTCGTGGTGTCCCTGACCACATCTAAGTTCT
CTAGCGTGCGGAACCAGTTTTGGTTCTCCGGCGCCATGATGATCATCACCGGCTATATCGGCCAGTTTTACGAGGTGTCTAATCTGACAGCCTTCCTGGTGTGGGGCGCCATCTCCTCTGCCTTCTTTTTCCACA
TCCTGTGGGTCATGAAGAAAGTGATCAACGAGGGCAAGGAGGGAATCTCTCCAGCAGGCCAGAAGATCCTGAGCAACATCTGGATTCTGTTCCTGATCAGCTGGACCCTGTACCCCGGCGCCTATCTGATGCC
TTACCTGACAGGCGTGGACGGCTTCCTGTACTCCGAGGATGGCGTGATGGCAAGGCAGCTGGTGTATACCATCGCCGACGTGAGCTCCAAAGTGATCTACGGCGTGCTGCTGGGCAATCTGGCAATCACCCT
GTCAAAAAACAAGGAACTGGTGGAGGCAAATAGCAAGAGCAGGATCACCAGCGAGGGCGAGTACATCCCCCTGGACCAGATCGACATCAACGTGGTGAGCAAGGGCGAGGAGCTGTTCACCGGGGTGGTG
CCCATCCTGGTCGAGCTGGACGGCGACGTAAACGGCCACAAGTTCAGCGTGTCCGGCGAGGGCGAGGGCGATGCCACCTACGGCAAGCTGACCCTGAAGTTCATCTGCACCACCGGCAAGCTGCCCGTGCCC
TGGCCCACCCTCGTGACCACCTTCGGCTACGGCCTGCAGTGCTTCGCCCGCTACCCCGACCACATGAAGCAGCACGACTTCTTCAAGTCCGCCATGCCCGAAGGCTACGTCCAGGAGCGCACCATCTTCTTCAA
GGACGACGGCAACTACAAGACCCGCGCCGAGGTGAAGTTCGAGGGCGACACCCTGGTGAACCGCATCGAGCTGAAGGGCATCGACTTCAAGGAGGACGGCAACATCCTGGGGCACAAGCTGGAGTACAAC
TACAACAGCCACAACGTCTATATCATGGCCGACAAGCAGAAGAACGGCATCAAGGTGAACTTCAAGATCCGCCACAACATCGAGGACGGCAGCGTGCAGCTCGCCGACCACTACCAGCAGAACACCCCCATC
GGCGACGGCCCCGTGCTGCTGCCCGACAACCACTACCTGAGCTACCAGTCCGCCCTGAGCAAAGACCCCAACGAGAAGCGCGATCACATGGTCCTGCTGGAGTTCGTGACCGCCGCCGGGATCACTCTCGGC
ATGGACGAGCTGTACAAGTTCTGCTACGAGAACGAGGTGTGA

eKR2 = C2C1-KR2-TS-eYFP-ER (ND7/23-cells):

ATGGACTATGGGGGAGCACTGTCCGCCGTCGGGCTGTTTCAGACTTCCTACACCCTGGAGAACAACGGGAGCGTCATTTGCATTCCTAACAATGGCCAGTGCTTCTGTCTGGCCTGGCTGAAGAGCAACGGGA
CCCAGGAACTGGGCAATGCCAACTTTGAGAATTTCATCGGCGCCACCGAGGGCTTTAGCGAGATCGCCTATCAGTTCACCTCCCACATCCTGACACTGGGCTATGCCGTGATGCTGGCCGGCCTGCTGTACTTT
ATCCTGACAATCAAGAACGTGGACAAGAAGTTCCAGATGTCTAATATCCTGAGCGCCGTGGTCATGGTGAGCGCCTTCCTGCTGCTGTATGCCCAGGCCCAGAACTGGACCAGCTCCTTTACATTCAATGAGG
AAGTGGGCAGGTACTTTCTGGACCCATCCGGCGATCTGTTCAACAATGGCTACAGATATCTGAACTGGCTGATCGATGTGCCCATGCTGCTGTTTCAGATCCTGTTCGTGGTGTCCCTGACCACATCTAAGTTCT
CTAGCGTGCGGAACCAGTTTTGGTTCTCCGGCGCCATGATGATCATCACCGGCTATATCGGCCAGTTTTACGAGGTGTCTAATCTGACAGCCTTCCTGGTGTGGGGCGCCATCTCCTCTGCCTTCTTTTTCCACA
TCCTGTGGGTCATGAAGAAAGTGATCAACGAGGGCAAGGAGGGAATCTCTCCAGCAGGCCAGAAGATCCTGAGCAACATCTGGATTCTGTTCCTGATCAGCTGGACCCTGTACCCCGGCGCCTATCTGATGCC
TTACCTGACAGGCGTGGACGGCTTCCTGTACTCCGAGGATGGCGTGATGGCAAGGCAGCTGGTGTATACCATCGCCGACGTGAGCTCCAAAGTGATCTACGGCGTGCTGCTGGGCAATCTGGCAATCACCCT
GTCAAAAAACAAGGAACTGGTGGAGGCAAATAGCGCAGCACCGGTAAAGAGCAGGATCACCAGCGAGGGCGAGTACATCCCCCTGGACCAGATCGACATCAACGTGGTGAGCAAGGGCGAGGAGCTGTTC
ACCGGGGTGGTGCCCATCCTGGTCGAGCTGGACGGCGACGTAAACGGCCACAAGTTCAGCGTGTCCGGCGAGGGCGAGGGCGATGCCACCTACGGCAAGCTGACCCTGAAGTTCATCTGCACCACCGGCAA
GCTGCCCGTGCCCTGGCCCACCCTCGTGACCACCTTCGGCTACGGCCTGCAGTGCTTCGCCCGCTACCCCGACCACATGAAGCAGCACGACTTCTTCAAGTCCGCCATGCCCGAAGGCTACGTCCAGGAGCGCA
CCATCTTCTTCAAGGACGACGGCAACTACAAGACCCGCGCCGAGGTGAAGTTCGAGGGCGACACCCTGGTGAACCGCATCGAGCTGAAGGGCATCGACTTCAAGGAGGACGGCAACATCCTGGGGCACAAG
CTGGAGTACAACTACAACAGCCACAACGTCTATATCATGGCCGACAAGCAGAAGAACGGCATCAAGGTGAACTTCAAGATCCGCCACAACATCGAGGACGGCAGCGTGCAGCTCGCCGACCACTACCAGCAG
AACACCCCCATCGGCGACGGCCCCGTGCTGCTGCCCGACAACCACTACCTGAGCTACCAGTCCGCCCTGAGCAAAGACCCCAACGAGAAGCGCGATCACATGGTCCTGCTGGAGTTCGTGACCGCCGCCGGG
ATCACTCTCGGCATGGACGAGCTGTACAAGTTCTGCTACGAGAACGAGGTGTGA

KR2-TEV-6xHis (*E.coli*):

ATGACGCAGGAACTGGGCAACGCCAACTTTGAAAACTTTATCGGTGCAACGGAAGGCTTTAGCGAAATCGCATACCAATTCACGAGCCATATCCTGACCCTGGGCTACGCAGTTATGCTGGCTGGTCTGCTGT
ATTTCATTCTGACGATCAAAAACGTCGATAAAAAATTCCAGATGAGCAACATCCTGTCTGCAGTGGTTATGGTTTCTGCTTTCCTGCTGCTGTACGCGCAGGCCCAAAACTGGACCAGCTCTTTCACGTTTAATG
AAGAAGTGGGCCGTTATTTCCTGGATCCGAGCGGCGACCTGTTTAACAATGGTTATCGCTACCTGAACTGGCTGATCGACGTTCCGATGCTGCTGTTCCAGATTCTGTTTGTCGTGAGTCTGACCACGTCCAAA
TTTAGTTCCGTGCGTAACCAGTTCTGGTTTAGCGGCGCAATGATGATTATCACCGGCTACATTGGTCAATTCTATGAAGTCTCTAATCTGACGGCTTTTCTGGTGTGGGGTGCGATCTCATCGGCCTTTTTCTTTC
ACATTCTGTGGGTTATGAAGAAAGTGATTAACGAAGGCAAAGAAGGTATCTCACCGGCGGGTCAGAAAATTCTGTCGAATATTTGGATCCTGTTCCTGATCAGTTGGACCCTGTATCCGGGCGCCTACCTGAT
GCCGTATCTGACCGGCGTGGATGGTTTTCTGTATAGTGAAGACGGTGTGATGGCGCGCCAACTGGTTTACACCATCGCCGATGTGAGCTCCAAAGTTATTTATGGCGTCCTGCTGGGTAATCTGGCGATTACCC
TGAGCAAAAACAAAGAACTGGTGGAAGCGAACAGCGAAAATCTGTACTTCCAAGGTCTCGAGCACCACCACCACCACCACTGA

Supplementary Figure 4:

Composition of all buffers used for oocytes and ND7/23-cells

extracellular buffer oocytes	composition [mM]	pH (adjusted with)
Na 10.0	NaCl [100], $MgCl_2$ [1.0], $CaCl_2$ [0.1], glycine [5]	10.0 (NaOH)
Na 7.5	NaCl [100], $MgCl_2$ [1.0], $CaCl_2$ [0.1], MOPS [5]	7.5 (NaOH)
Na 5.0	NaCl [100], $MgCl_2$ [1.0], $CaCl_2$ [0.1], citric acid/Na-citrate [5]	5.0 (NaOH)
KCl 10.0	KCl [100], $MgCl_2$ [1.0], $CaCl_2$ [0.1], glycine [5]	10.0 (KOH)
KCl 7.5	KCl [100], $MgCl_2$ [1.0], $CaCl_2$ [0.1], MOPS [5]	7.5 (KOH)
KCl 5.0	KCl [100], $MgCl_2$ [1.0], $CaCl_2$ [0.1], citric acid [5]	5.0 (KOH)
LiCl 10.0	LiCl [100], $MgCl_2$ [1.0], $CaCl_2$ [0.1], glycine [5]	10.0 (LiOH)
LiCl 7.5	LiCl [100], $MgCl_2$ [1.0], $CaCl_2$ [0.1], MOPS [5]	7.5 (LiOH)
LiCl 5.0	LiCl [100], $MgCl_2$ [1.0], $CaCl_2$ [0.1], citric acid [5]	5.0 (LiOH)
50/50 NaCl/KCl	NaCl [50], KCl [50], $MgCl_2$ [1.0], $CaCl_2$ [0.1], glycine [5]	10.0 (NaOH)
50 KCl	KCl [50], $MgCl_2$ [1.0], $CaCl_2$ [0.1], glycine [5]	10.0 (KOH)
KCl 10.0 (titration)	KCl [200/100/50/25/10/0], glucose [0/0/50/75/90/100], $MgCl_2$ [1.0], $CaCl_2$ [0.1], glycine [5]	10.0 (KOH)
NMG 10.0	NMG [100], $MgCl_2$ [1.0], $CaCl_2$ [0.1], glycine [5]	10.0 (HCl)
NMG 7.5	NMG [100], $MgCl_2$ [1.0], $CaCl_2$ [0.1], MOPS [5]	7.5 (HCl)
Na-Gluk 10.0	Na-gluconate [100], $MgCl_2$ [1.0], $CaCl_2$ [0.1], glycine [5]	10.0 (NaOH)
Na-Gluk 7.5	Na-gluconate [100], $MgCl_2$ [1.0], $CaCl_2$ [0.1], MOPS [5]	7.5 (NaOH)
$MgCl_2$ 7.5	$MgCl_2$ [100], $CaCl_2$ [0.1], MOPS [5]	10.0 (NaOH)
$CaCl_2$ 7.5	$MgCl_2$ [1.0], $CaCl_2$ [100], MOPS [5]	7.5 (NaOH)

extracellular buffer ND7/23-cells	composition [mM]	pH (adjusted with)	osmolarity (adjusted with glucose)
NaCl 9.0	NaCl [110], KCl [1], $MgCl_2$ [1.0], $CaCl_2$ [1.0], Tris [10], TEA [20], CsCl [5], $BaCl_2$ [5]	9.0 (HCl)	310 mOsm
KCl 9.0	NaCl [1], KCl [110], $MgCl_2$ [1.0], $CaCl_2$ [1.0], Tris [10], TEA [20], CsCl [5], $BaCl_2$ [5]	9.0 (HCl)	310 mOsm
LiCl 9.0	NaCl [1], KCl [1], LiCl [110], $MgCl_2$ [1.0], $CaCl_2$ [1.0], Tris [10], TEA [20], CsCl [5], $BaCl_2$ [5]	9.0 (HCl)	310 mOsm

intracellular buffer ND7/23-cells	composition [mM]	pH (adjusted with)	osmolarity (adjusted with glucose)
0.1 mM NaCl 0.1 mM KCl pH 7.2	NaCl [0.1], KCl [0.1], NMG [110], $MgCl_2$ [1.0], $CaCl_2$ [1.0], EGTA [10], HEPES [10]	7.2 (HCl)	290 mOsm
1 mM NaCl 1 mM KCl pH 7.2	NaCl [1], KCl [1], NMG [110], $MgCl_2$ [1.0], $CaCl_2$ [1.0], EGTA [10], HEPES [10]	7.2 (HCl)	290 mOsm
110 mM NaCl 1 mM KCl pH 7.2	NaCl [110], KCl [1], $MgCl_2$ [1.0], $CaCl_2$ [1.0], EGTA [10], HEPES [10]	7.2 (NaOH)	290 mOsm
1 mM NaCl 110 mM KCl pH 7.2	NaCl [1], KCl [110], $MgCl_2$ [1.0], $CaCl_2$ [1.0], EGTA [10], HEPES [10], TEA [20], CsCl [5], $BaCl_2$ [5]	7.2 (KOH)	290 mOsm
1 mM NaCl 1 mM KCl 110 mM LiCl pH 7.2	NaCl [1], KCl [1], LiCl [110], $MgCl_2$ [1.0], $CaCl_2$ [1.0], EGTA [10], HEPES [10]	7.2 (LiOH)	290 mOsm

Supplementary Figure 5

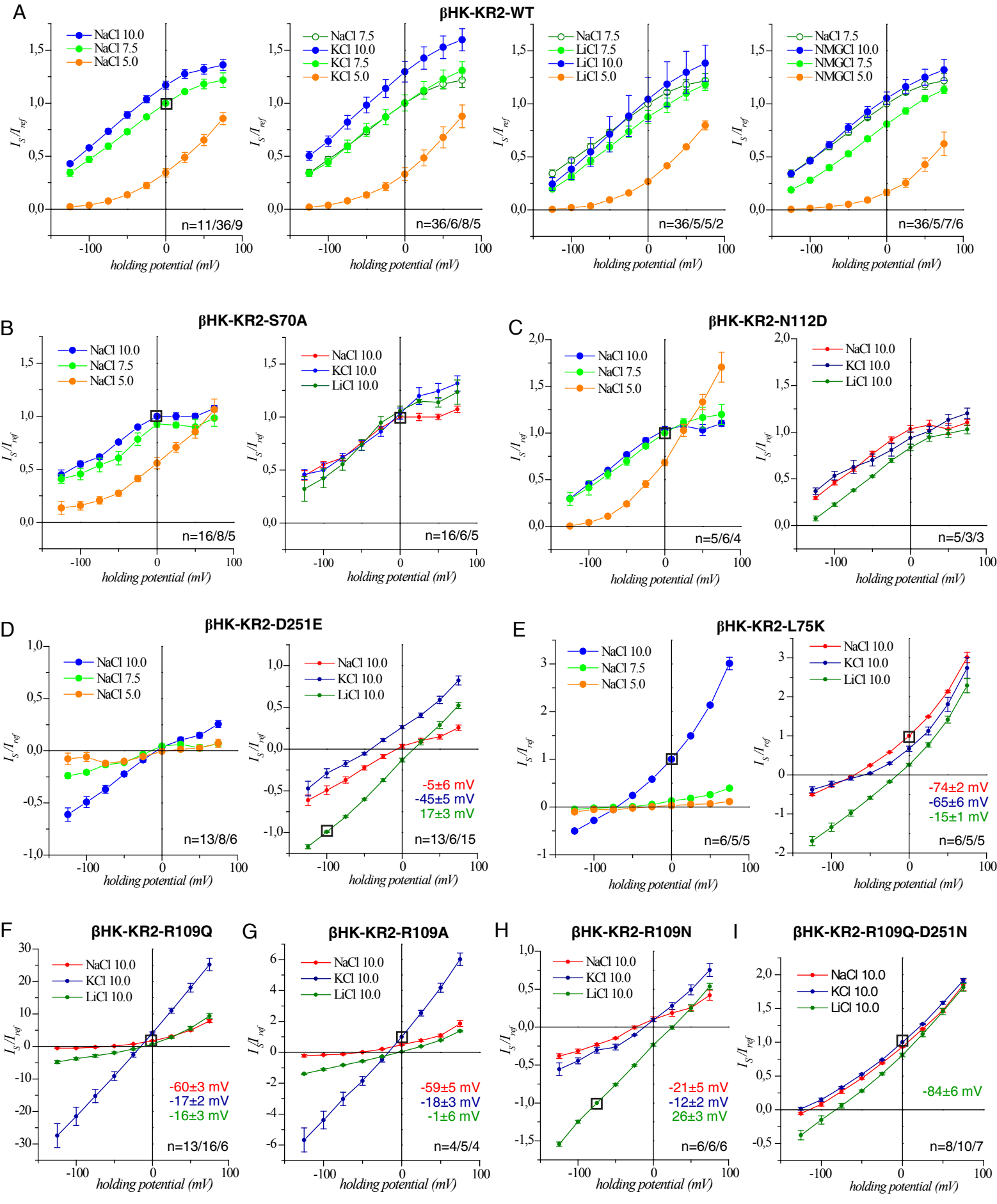

Supplementary Figure 5: Current-voltage plots for various KR2 mutants, measured in *Xenopus laevis* oocytes. Cells were measured at different pH_o values or cation conditions. Reversal potentials are indicated, if possible, and where appropriate. Small black boxes show the respective condition used for normalization.

Supplementary Figure 6

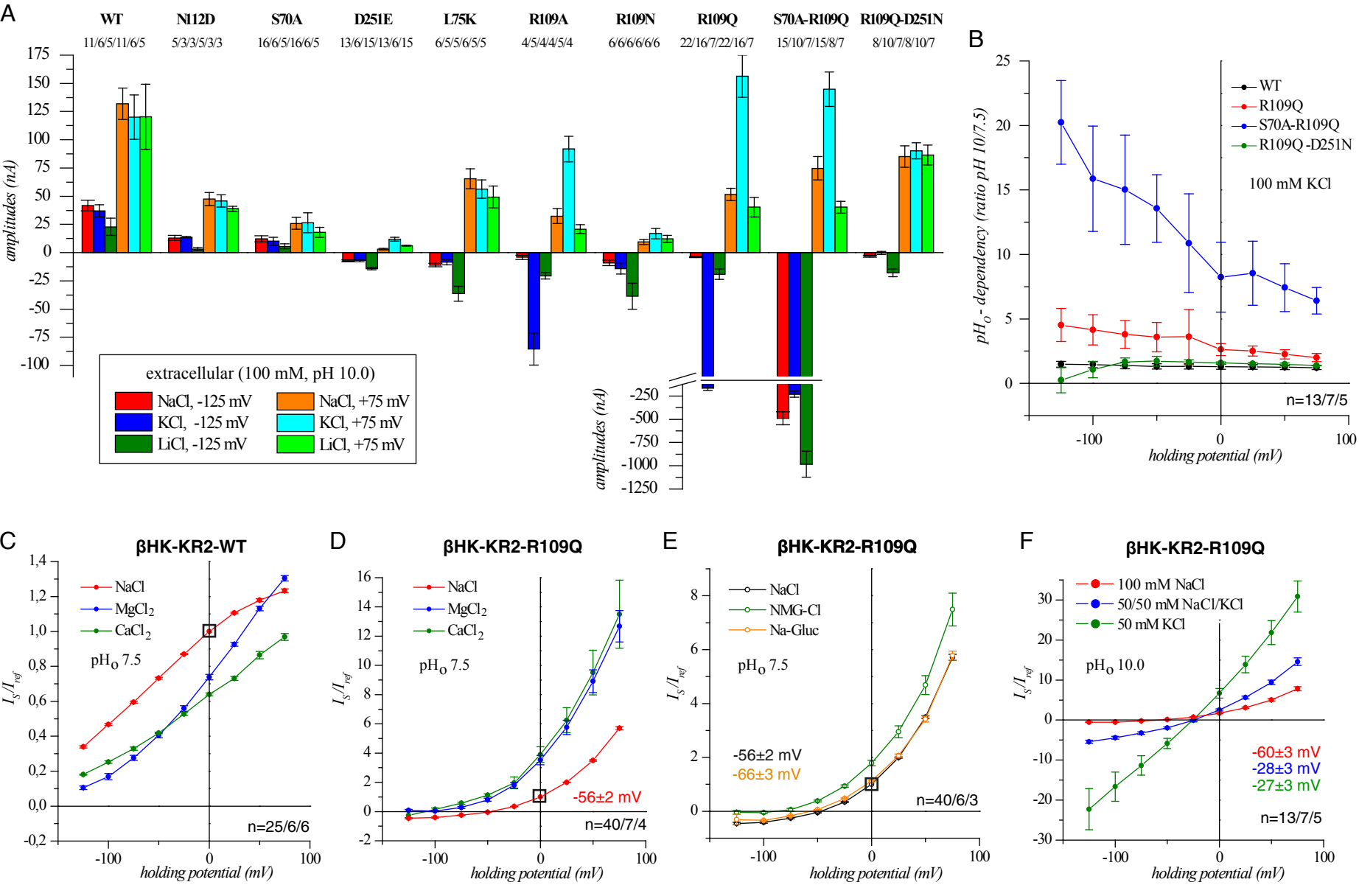

Supplementary Figure 6: Additional results obtained from electrophysiological measurements in oocytes. (*A*) Comparison of the absolute stationary photocurrent amplitudes for different extracellular buffer conditions and holding potentials. The mutants D116N and D251N are not shown because no obvious stationary photocurrents were observed. (*B*) The pH_o-dependency is illustrated as the ratio between the photocurrents at pH_o 10.0 and pH_o 7.5 (with 100 mM KCl). Current-voltage plots for (*C*) KR2-WT and (*D-E*) KR2-R109Q at different extracellular ion conditions (all at a concentration of 100 mM). Ca^{+2} and Mg^{+2} are not transported but influence the photocurrents, whereas removal of extracellular Cl^- does not influence photocurrents. Data indicate minor passive Na^+ conductance. Small black boxes show the respective condition used for normalization. (*F*) Current-voltage-plot of KR2-R109Q in different extracellular Na^+ and K^+ concentrations, illustrating the competition between Na^+ and K^+(photocurrents were normalized to 100 mM NaCl, pH_o 7.5, not shown in this plot). K^+determines the reversal potential, whereas Na^+ shows an inhibitory effect.

Supplementary Figure 7

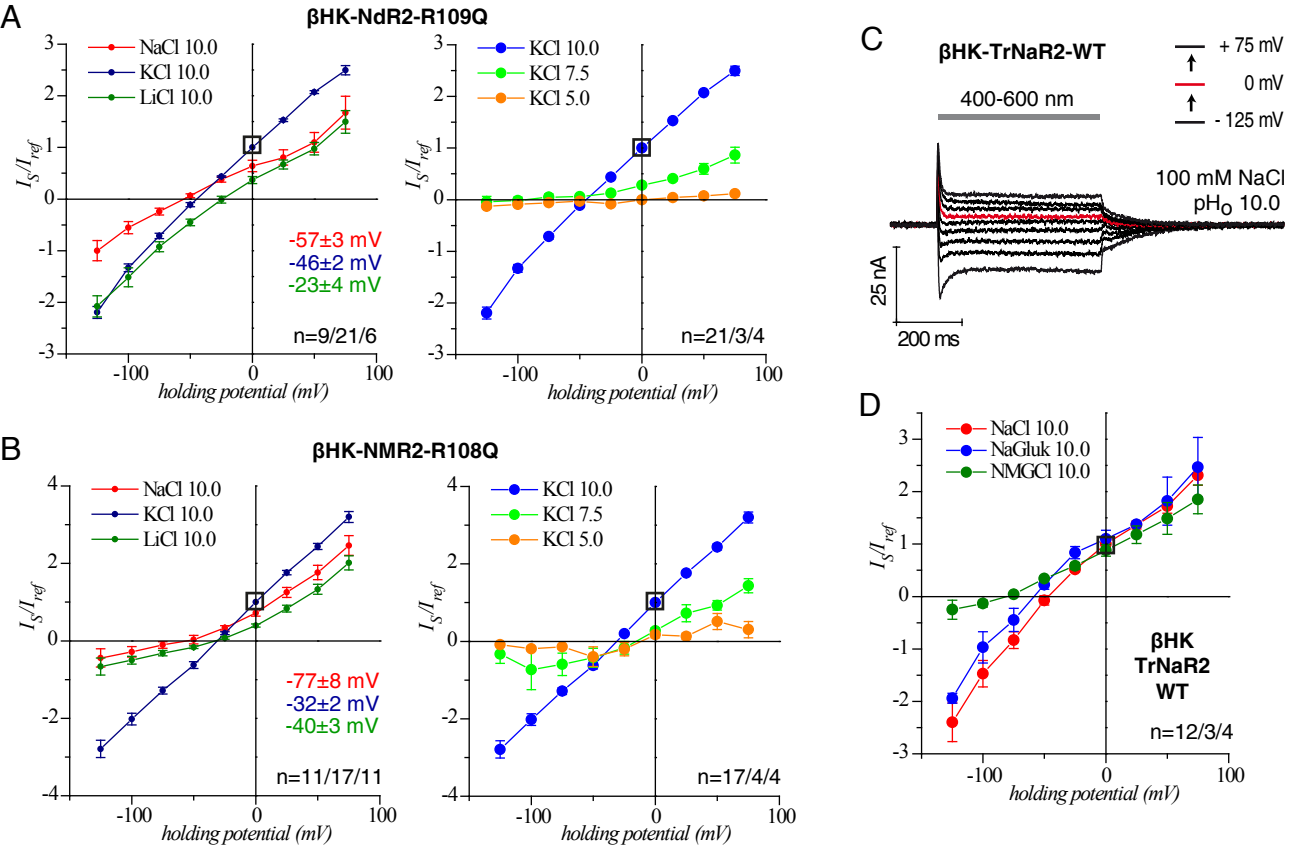

Supplementary Figure 7: Further electrophysiological analysis of NdR2βHK-R109Q, NMR2βHK-R108Q, and TrNaR2βHK-WT in oocytes. (*A-B*) Current-voltage plots of NdR2βHK-R109Q and NMR2βHK-R108Q demonstrate different ion-selectivities of the mutants and their pHo-dependency (normalized to 100 mM KCl, pHo 10, and 0 mV). (*C*) Photocurrent traces of TrNaR2βHK-WT indicate leakiness in the WT protein. However, amplitudes were poor, and only the best measurement is shown. (*D*) Current-voltage plot of TrNaR2βHK-WT after removal of Cl^-or Na^+ ions (normalized to 100 mM NaCl, pHo 10, and 0 mV. Results indicate leakiness for cations.

Supplementary Figure 8

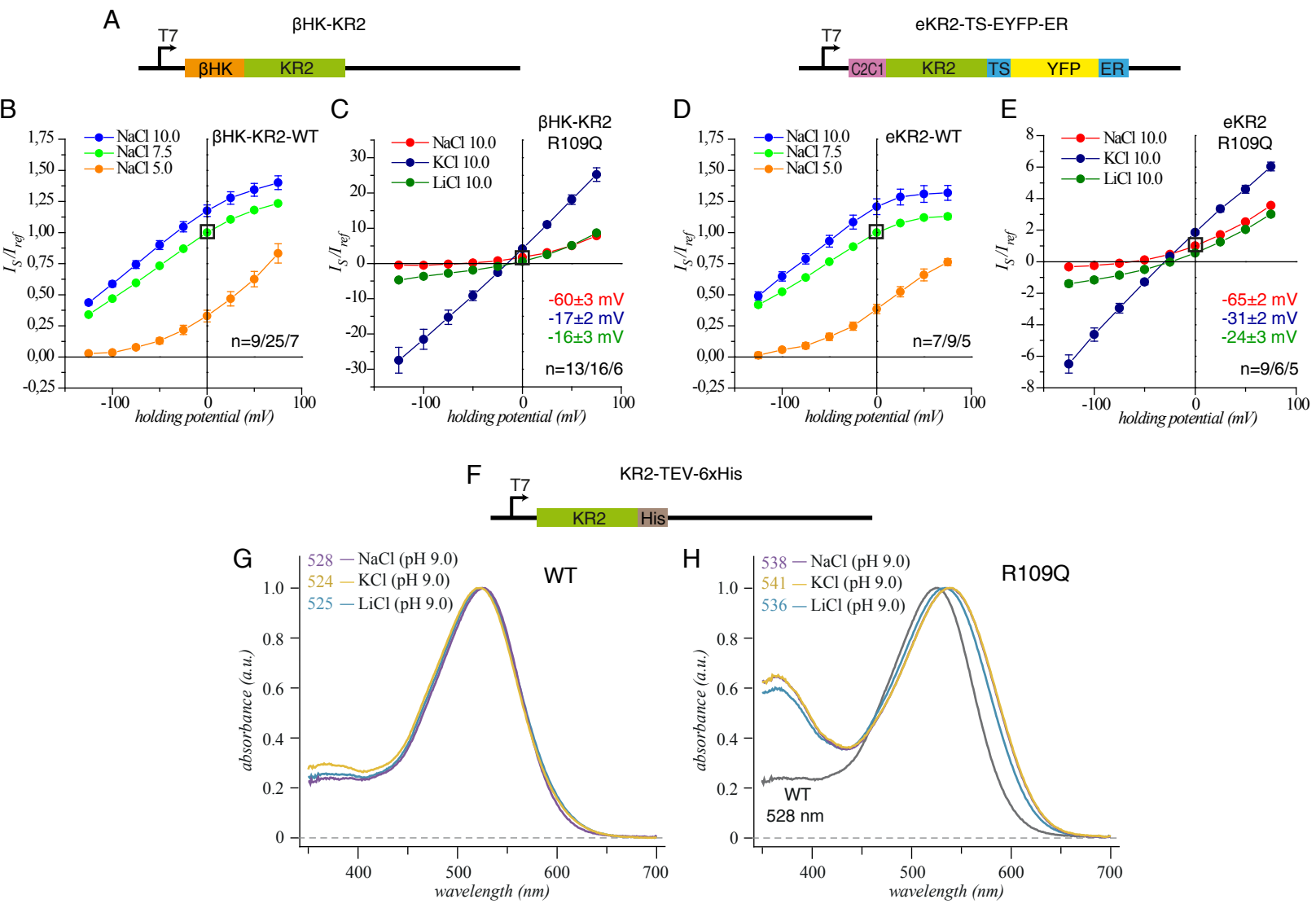

Supplementary Figure 8: Influence of construct design and spectral characteristics of KR2. (*A*) Structure of the targeting constructs KR2βHK and eKR2; nucleotide sequences of each construct are shown in Supplementary Fig. 3. (*B-E*) Comparison of the two targeting constructs, both tested in oocytes, for KR2-WT and KR2-R109Q. Photocurrents were normalized to 0 mV, 100 mM NaCl, and pH 7.5 (WT) or pH 10.0 (R109Q). The pH_o-dependency was similar for all constructs, but differences in the reversal potentials were observed for KR2-R109Q. (*F*) The constructs utilized for the pH-assay and for purification from *E. coli* are functional without any additional targeting. (*G-H*) Absorption spectra of purified KR2-WT and KR2-R109Q, measured at pH 9.0 and in 110 mM of the indicated salt. KR2-R109Q is characterized by an increased amount of protein with a deprotonated Schiff-base (365 nm) and an increased cation-dependency of the absorption maxima.

Supplementary Figure 9

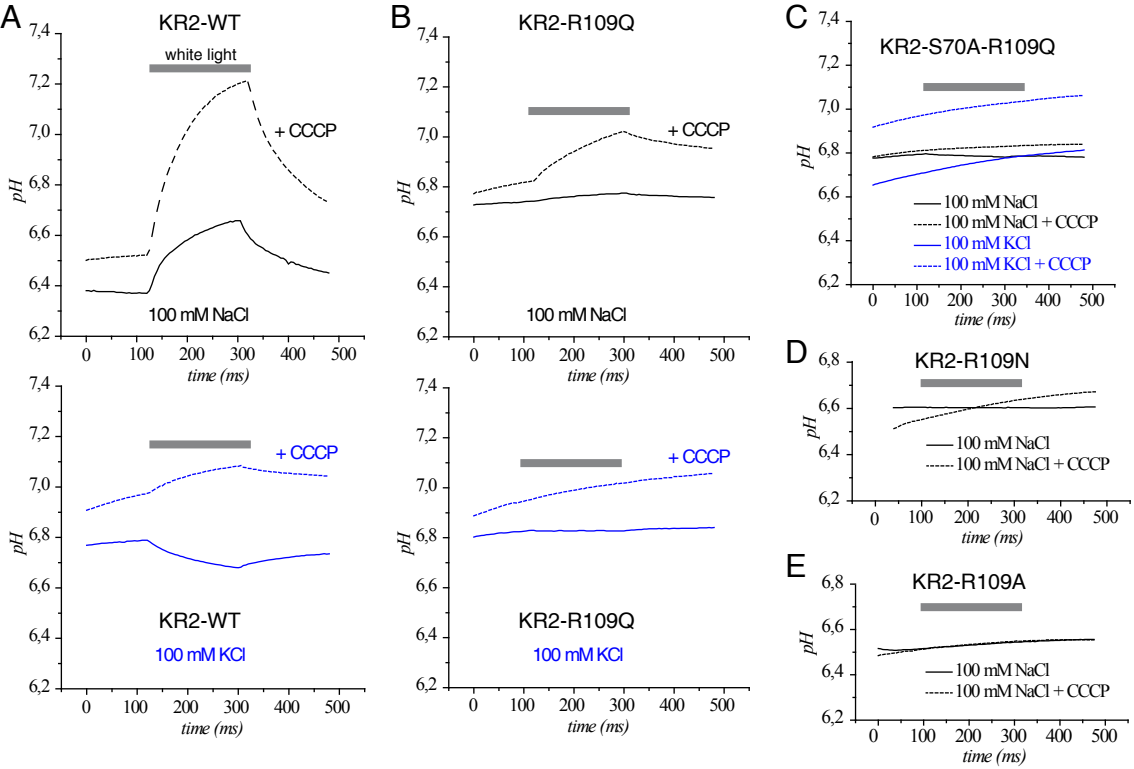

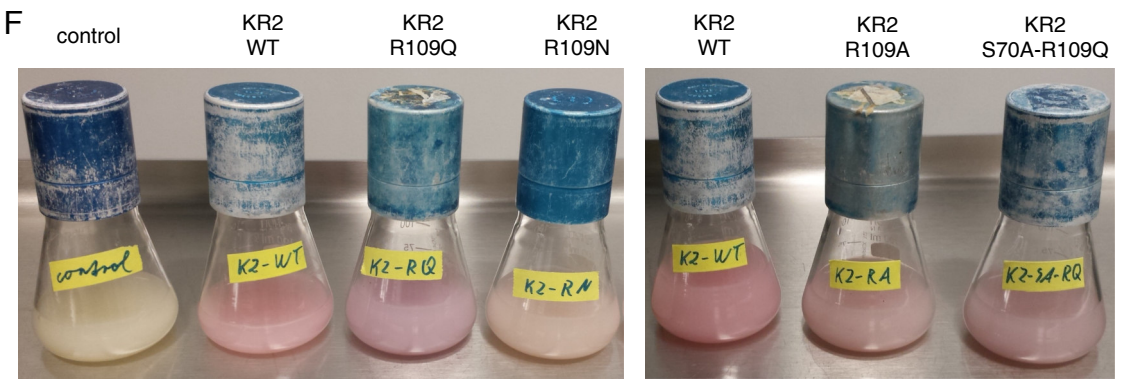

Supplementary Figure 9: Analysis of light-induced pH changes in suspensions of *Escherichia coli* expressing various KR2 mutants. Suspensions of cells expressing (*A*) KR2-WT, (*B, D-E*) KR2-R109Q/N/A, and (*C*) KR2-S70A-R109Q were tested before (continuous line) and after (dotted lines) addition of the protonophore, carbonyl cyanide m-chlorophenyl hydrazone (CCCP). Only WT and R109Q KR2 exhibited pH-changes during illumination. (*F*) Photos *E. coli* cell cultures are shown (all concentrated to OD_{600} =10). The faint colors of KR2-R109N, KR2-R109Q, and KR2-S70A-R109Q indicate lower protein expression.

Supplementary Figure 10:

Overview of all KR2 constructs and mutants tested in oocytes

	location/motivation/earlier investigations in KR2	**results**
KR2-WT	/	only positive currents
βKR2-WT	/	only positive currents
eKR2-WT	/	only positive currents
βKR2-L32E	extracellular half channel, interaction partner of R109	positive currents + negative currents with K and Li at high elechtrochemical load (-125 mV)
βKR2-S60T	ion uptake region	only positive currents
βKR2-N61P	ion uptake region, increased proton pumping proposed by Kato et al. 2015 (N61Y), Gushchin et al. 2015 (N61M)	only positive currents
βKR2-S64T	ion uptake region	only positive currents
βKR2-S70A	counter-ion complex, Kato 2015 et al. (S70T/A)	studied intensively in this study
βKR2-S70V	counter-ion complex, Kato 2015 et al. (S70T/A)	similar to S70A
βKR2-L75K	counter-ion complex, Inoue et al. 2013 (R109A)	studied intensively in this study
βKR2-R109Q	counter-ion complex, Inoue et al. 2013 (R109A)	studied intensively in this study
βKR2-R109A	counter-ion complex, Inoue et al. 2013 (R109A)	studied intensively in this study
βKR2-R109N	counter-ion complex, Inoue et al. 2013 (R109A)	studied intensively in this study
βKR2-N112D	counter-ion complex, Inoue et al. 2013 (N112A/D)	studied intensively in this study
βKR2-D116N	counter-ion complex, Inoue et al. 2013 (D116A/E/N)	studied intensively in this study
βKR2-D116E	counter-ion complex, Inoue et al. 2013 (D116A/E/N)	only positive currents, low amplitudes
βKR2-Q244E	ion-release cavity, interaction partner of R109	only positive currents
βKR2-D251N	counter-ion complex, Inoue et al. 2013 (D251A/E/N)	studied intensively in this study
βKR2-D251E	counter-ion complex, Inoue et al. 2013 (D251A/E/N)	studied intensively in this study
βKR2-G263W	ion uptake region, increased potassium pumping proposed by Kato et al. 2015 (G263W) and Gushchin et al. 2015 (G263F/G263L)	only positive currents
βKR2-N61P-G263W	ion uptake region, increased potassium pumping proposed by Kato et al. 2015	only positive currents, low amplitudes, pronounced transient peak current
βKR2-R109Q-E11D	ion-release cavity, Gushchin et al. 2015 (E11A), Kato et al. 2015 (E11A)	leaky , low amplitudes
βKR2-R109Q-E18Q	extracellular side	leaky , low amplitudes
βKR2-R109Q-F20A	ion-release cavity	leaky , low amplitudes
βKR2-R109Q-E22Q	extracellular side	similar to R109Q

βKR2-R109Q-T33D	transmembrane surface of KR2	very low amplitudes
βKR2-R109Q-V67A	interaction with Schiff-base from intracellular side	leaky for Na/K/Li, high amplitudes (but lower than R109Q-S70A)
βKR2-R109Q-S70A	see single mutations	studied intensively in this study
βKR2-R109Q-S70V	see single mutations	similar to R109Q-S70A but lower amplitudes
βKR2-R109Q-L75K	see single mutations	similar to R109Q
βKR2-R109Q-L75T	see single mutations	leaky for Na/K/Li, low amplitudes
βKR2-R109Q-E91Q	extracellular side	leaky , low amplitudes
βKR2-R109Q-R94Q	extracellular side	leaky , low amplitudes
βKR2-R109Q-D98N	extracellular side	leaky
βKR2-R109Q-D102N	extracellular side, Gushchin et al. 2015 (D102N), Kato et al. 2015 (D102N)	leaky
βKR2-R109Q-N112D	see single mutations	similar to R109Q leaky
βKR2-R109Q-D116N	see single mutations	no stationary currents
βKR2-R109Q-D116E	see single mutations	leaky, very low amplitudes
βKR2-R109Q-D116A	see single mutations	no stationary currents
βKR2-R109Q-L120D	interaction with Schiff-base from intracellular side	no currents
βKR2-R109Q-Q123A	ion uptake region, Inoue et al. 2013 (Q123A/E/D)	leaky, low amplitudes
βKR2-R109Q-E160Q	ion-release cavity, Inoue et al. (E160Q), Gushchin et al. 2015 (E160A), Kato et al. 2015 (E160A)	leaky
βKR2-R109Q-E237Q	extracellular side	leaky
βKR2-R109Q-R243Q	ion-release cavity, Gushchin et al. 2015 (R243Q/A), Kato et al. 2015 (R243A)	leaky, low amplitudes
βKR2-R109Q-D251N	see single mutations	studied intensively in this study
βKR2-R109Q-D251E	see single mutations	leaky for Na/K/Li, low amplitudes, pH_o-dependency further increased
βKR2-R109Q-D251T	see single mutations	very low amplitudes
βKR2-R109Q-D251H	see single mutations	very low amplitudes
ßKR2-R109Q-S254D	interaction with Schiff-base from intracellular side	no currents
βKR2-R109Q-S70A-L75K	see single mutations	leakyness for Na/K/Li, very high amplitudes for Li
βKR2-R109Q-N112D-D251N	see single mutations	no stationary currents
βKR2-R109Q-N61P-G263W	see single mutations	no currents
eKR2-R109A	see single mutations	studied intensively in this study
eKR2-R109Q	see single mutations	studied intensively in this study
eKR2-R109Q-S70A	see single mutations	studied intensively in this study